Cancer Letters 616 (2025) 217565

Contents lists available at ScienceDirect

Cancer Letters

journal homepage: www.elsevier.com/locate/canlet

Original Articles

mTOR-mediated p62/SQSTM1 stabilization confers a robust survival mechanism for ovarian cancer

Tomohiro Tamura [a,b,#], Shimpei Nagai [a,#], Kenta Masuda [a,*], Keiyo Imaeda [a], Eiji Sugihara [c], Juntaro Yamasaki [c], Miho Kawaida [d], Yuji Otsuki [c], Kentaro Suina [e,f], Hiroyuki Nobusue [c], Tomoko Akahane [a,1], Tatsuyuki Chiyoda [a], Iori Kisu [a], Yusuke Kobayashi [a,2], Kouji Banno [a,3], Kazuhiro Sakurada [b], Hajime Okita [d], Rui Yamaguchi [g,h], Ahmed Ashour Ahmed [i,j,k,l], Wataru Yamagami [a], Hideyuki Saya [c], Daisuke Aoki [a,4,5], Osamu Nagano [c]

[a] Department of Obstetrics and Gynecology, Keio University School of Medicine, Tokyo, Japan
[b] Department of Extended Intelligence for Medicine, The Ishii-Ishibashi Laboratory, Keio University School of Medicine, Tokyo, Japan
[c] Division of Gene Regulation, Oncology Innovation Center, Fujita Health University, Toyoake, Japan
[d] Division of Diagnostic Pathology, Keio University Hospital, Tokyo, Japan
[e] Department of Neurosurgery, Yale School of Medicine, New Haven, CT, USA
[f] Department of Respiratory Medicine, Juntendo University Graduate School of Medicine, Tokyo, Japan
[g] Division of Cancer Systems Biology, Aichi Cancer Center Research Institute, Nagoya, Japan
[h] Division of Cancer Informatics, Nagoya University Graduate School of Medicine, Nagoya, Japan
[i] Ovarian Cancer Cell Laboratory, MRC Weatherall Institute of Molecular Medicine, University of Oxford, Oxford, OX3 9DS, UK
[j] Nuffield Department of Women's & Reproductive Health, University of Oxford, Oxford, OX3 9DU, UK
[k] Department of Gynecological Oncology, Churchill Hospital, Oxford University Hospitals, Oxford, OX3 7LE, UK
[l] Oxford NIHR Biomedical Research Centre, Oxford, OX4 2PG, UK

ARTICLE INFO

Keywords:
Ovarian cancer
p62/SQSTM1
mTOR inhibitor
BRCA1/2 wild type

ABSTRACT

Over 50 % of patients with high-grade serous carcinoma (HGSC) are homologous recombination proficient, making them refractory to platinum-based drugs and poly (ADP-ribose) polymerase (PARP) inhibitors. These patients often develop progressive resistance within 6 months after primary treatment and tend to die early, thus new therapies are urgently needed. In this study, we comprehensively investigated this tumor type by leveraging a combination of machine learning analysis of a large published dataset and newly developed genetically engineered HGSC organoid models from murine fallopian tubes. Aberrant activation of RAS/PI3K signaling was a signature of poor prognosis in *BRCA1/2* wild-type ovarian cancer, and mTOR-induced elevated p62 expression was a robust marker of chemotherapy-induced mTOR-p62-NRF2 signal activation. mTOR inhibition with everolimus decreased p62 and enhanced sensitivity to conventional chemotherapy, indicating that p62 serves as an important biomarker for therapeutic intervention. Combination therapy with conventional chemotherapy and mTOR inhibitors is a promising therapeutic strategy for refractory HGSC, with p62 as a biomarker.

* Corresponding author. Department of Obstetrics and Gynecology, Keio University School of Medicine., 35 Shinanomachi, Shinjuku-ku, Tokyo, 160-8582, Japan.
E-mail address: ma-su-ken.a2@keio.jp (K. Masuda).
[1] Present address: Department of Pathology and Cytology, Faculty of Clinical Laboratory Sciences, Nitobe Bunka College, Tokyo, Japan.
[2] Present address: Department of Obstetrics and Gynecology, Institute of Medicine, University of Tsukuba, Ibaraki, Japan.
[3] Present address: Center of Maternal-Fetal/Neonatal Medicine, Hiroshima University Hospital, Hiroshima, Japan.
[4] Present address: Akasaka Sannou Medical Center, Tokyo, Japan.
[5] Present address: International University of Health and Welfare Graduate School, Tokyo, Japan.
[#] Co-first author.

https://doi.org/10.1016/j.canlet.2025.217565
Received 22 November 2024; Received in revised form 14 February 2025; Accepted 14 February 2025
Available online 17 February 2025

1. Introduction

High-grade serous carcinoma (HGSC) is the most common subtype of epithelial ovarian cancer and is characterized by aggressive proliferation and difficulty in its early detection, resulting in poor progression due to recurrence and acquisition of chemoresistance in many cases [1,2]. Although the standard treatment of advanced HGSC has long been a combination of debulking surgery and chemotherapy, such as carboplatin (CBDCA) and paclitaxel (PTX), progress in personalized therapy based on the genetic profiles of each patient has been made. For instance, poly (ADP-ribose) polymerase (PARP) inhibitors, such as olaparib, have been shown to extend progression-free survival (PFS) and overall survival (OS) in patients with HGSC having *BRCA1/2* pathogenic variants, which cause homologous recombination deficiency (HRD) [3,4]. However, in patients with HGSC without *BRCA1/2* pathogenic variants, the survival benefit of olaparib is modest [5]. The Cancer Genome Atlas (TCGA) cohort, have also reported that patients with HGSC with *BRCA1/2* pathogenic variants showed a tendency for living longer than did those with *BRCA1/2* wild type (WT) [6–8]. This can be explained by the differences in sensitivity to platinum-based drugs. However, responses of patients with HGSC with *BRCA1*/2 WT to treatment vary and are heterogeneous, with some patients not relapsing for longer periods of time and others relapsing early or during treatment and being considered "refractory" cases. This suggests that some determinant factors other than *BRCA1/2* status convert patients with HGSC into refractory cases; however, no studies have explored these factors [9]. Thus, identifying the determining factor of the "refractoriness" of patients with HGSC and developing new remedies are urgently needed.

In addition, HGSCs are characterized by a high rate of recurrence, even though they respond well to chemotherapy. Thus, minimal residual disease (MRD) cannot be eliminated by chemotherapy; recurrence occurs when MRD regrows. Although there have been reports of ovarian cancer MRD, no treatment strategy for its clinical use has been developed [10].

In this study, we aimed to detect a poor prognostic signature in patients with *BRCA1*/2 WT ovarian cancer using a computational approach; investigate the background mechanism of the poor prognostic signature using newly developed syngeneic mouse models based on organoid technology. We also aimed to validate this with human clinical tumor samples, including pre- and post-chemotherapy samples; elucidate the nature of refractory HGSC and vulnerability of HGSC MRD; help identify potential therapeutic interventions for increasing sensitivity of refractory cases to chemotherapy and reducing recurrence risk in patients with HGSC.

2. Methods

2.1. Animal experiments

The mice were housed in an environmentally controlled room using a protocol approved by the University Institutional Animal Care and Use Committee with a project license of 20064. Normal fallopian tube epithelium organoids were established from the fallopian tube epithelium of $Rb1^{fl/fl}Trp53^{fl/fl}Myc^{LSL/LSL}$ mice (JAX Strain #029971, RRID: IMSR_JAX:029971) and $B6J.129(B6N)\text{-}Gt(ROSA)26Sor^{tm1(CAG\text{-}cas9^{*}_{/+}\text{-}EGFP)Fezh}/J$ mice (AX Strain #026175, RRID:IMSR_JAX:026175). BALB/cAJcl-nu/nu (RRID:IMSR_JCL:JCL:MID-0001) mice were used as recipients for the transplantation of fallopian tube epithelium organoid-derived tumor cells. Tumor cells were harvested via TrypLE and counted using trypan blue staining and a cell counter. Regarding in vivo characterization of the fallopian tube epithelium-derived tumor cells, 1×10^6 cells suspended in 150 μL of PBS were administered intraperitoneally (day 1). Considering in vivo treatment assay (Fig. 7b and c), 2×10^5 cells suspended in 50 μL of medium/Matrigel (1/2 v/v) were inoculated subcutaneously into each flank (day 1). The tumor volumes were measured every 3 days from day 7 using the following formula: V = (large tumor dimension) × (small tumor dimension)2 × π/6. CBDCA: 30 mg/kg i.p.; PTX: 8 mg/kg i.p.; everolimus: 5 mg/kg p.o., in principle.

2.2. TCGA ovarian cancer dataset analysis

RNA-sequence gene expression and survival data of TCGA ovarian cancer (422 cases, 429 files) were downloaded from the National Cancer Institute GDC Data Portal (https://portal.gdc.cancer.gov/). According to the clinical profiles, the data of the ovarian cancer patients who were followed up until death or a certain date, with IIIa or greater FIGO stages, were extracted and defined as the "WHOLE" (391 patients). On cBioPortal for cancer genomics (https://www.cbioportal.org/), we excluded patients with ovarian cancer with *BRCA1/2* mutations from genetically profiled WHOLE patients (258 patients) and defined the residues as "BRCA-WT" (202 patients). We used the log-scale normalized TPM values of each gene from a primary tumor file as gene expression data for transcriptomic analysis, in which chrY genes and genes with extremely low expression were excluded. We subsequently performed an R package "GSVA" (Humans; C5; BP; gene set sizes were 50–500) in the WHOLE patients and the BRCA-WT patients to score the activity of each pathway and allocated the patients into positive (or equal to 0) and negative groups according to each pathway score. Consequently, we calculated the p-values using Log-rank tests between the two groups for all analyzed pathways and ranked the pathways by the p-values.

2.3. Drugs

CBDCA, PTX, and olaparib are anticancer agents used to treat high-grade serous carcinomas. Everolimus is an allosteric mTORC1 inhibitor. Hydroxychloroquine is an autophagy inhibitor that prevents phagosome-lysosome fusion. Regarding in vitro cell culture studies, CBDCA (Sigma-Aldrich) and hydroxychloroquine (Sigma-Aldrich) were diluted in water, and PTX (Sigma-Aldrich), olaparib (CEM), and everolimus (CEM) were diluted in DMSO to the indicated concentrations. For the animal studies, paclitaxel was diluted in 5 % DMSO, 40 % polyethylene glycol #300, 5 % Tween 80, and 50 % water and stored in DMSO, and everolimus was diluted in 30 % propylene glycol, 5 % Tween 80, and 65 % water and stored in propylene glycol, in principle.

2.4. Organoid cultures and viral cell engineering

To establish normal fallopian tube epithelium organoids (cas-nFTE, nFTE), the fallopian tubes were dissected under a microscope, minced, and digested with collagenase type I at 37 °C, followed by incubation in TrypLE at 37 °C. Dispersed fallopian tube epithelial cells were mixed with Matrigel (Corning), and 20–25 μL drops of the matrix cell suspension were allowed to solidify on a 48-well plate at 37 °C. To stabilize the Matrigel, organoid medium was added. The organoid medium used was based on Advanced DMEM/F12 (Thermo Fisher Scientific) supplemented with 10 mM HEPES (Gibco), 2 mM GlutaMAX-I (Gibco), 50 × B27 (Gibco), 1 mM N-acetyl-L-cysteine (Sigma-Aldrich), R-spondin CM (JSR Life Science or In-house), Noggin CM (JSR Life Science or In-house), Afamin/Wnt3A CM (JSR Life Science), 50 ng/mL human EGF (Peprotech), and 500 nM A83-01 (Tocris), in principle. To add the first organoid medium at establishment or passage, the culture medium was supplemented with 10 μM Y-27632 (Sigma-Aldrich). To establish HGSC-modeling organoids, nFTE organoids were transfected with the pCMV-Cre plasmid (VectorBuilder, VB190701-1025ges) (cRPM) or infected with the Cre Lentiviral Vector (Enterobacteria phage P1) (pLenti-III) (Applied Biological Materials Inc.) (RPM). Approximately 2 days post-transfection or infection, the medium was replaced with a medium containing 10 μM Nutlin-3a (Selleck). cRPM cells stably expressing p62 or EGFP (mock) were established through lentiviral infection. The cDNAs encoding EGFP and human p62 (SQSTM1) were obtained from the DNASU Plasmid Repository (Arizona State University) and subcloned individually into the pLEX_307 lentiviral vector (RRID:

Addgene_41392). Tumor cells stably expressing GFP-LC3-mRuby3-LC3ΔG (a vector provided by N. Mizushima and H. Chino) were established through retroviral infection.

2.5. CRISPR/Cas9-mediated knockout of Trp53, Pten, Nf1, and Sqstm1

Briefly, cas-nFTE organoids were trypsinized, and the cells were collected in electroporation cuvettes (NepaGene) with OPTI-MEM, appropriate sgRNA, and the pCMV-Cre plasmid (VectorBuilder, VB190701-1025ges). Electroporation was performed using NEPA21 (NepaGene). After electroporation, the cells were incubated for 30 min, mixed with Matrigel, and covered with organoid medium containing 10 μM Y-27632. Approximately 2 days after transfection, the medium was exchanged with the medium containing 10 μM Nutlin-3a to select for *Trp53*-knockout organoids. sg*Trp53* RNA was synthesized using IDT Alt-R® CRISPR-Cas9 sgRNA *Trp53* AAGTCACAGCACATGACGG. sg*Pten*, sg*Nf1*, and sg*Sqstm1* RNAs were synthesized using FASMAC and then cloned into the lentiCRISPR v2 vector (Addgene plasmid #52961). For *Pten* knockout, the blasticidin resistance gene was subcloned into the lentiCRISPR v2 vector (RRID: Addgene_52961) using In-Fusion (Takara) according to the manufacturer's instructions. For *Nf1* knockout, the zeocin resistance gene was subcloned into the lentiCRISPR v2 vector. *Pten*-knocked RPM (RPMP), *Nf1*-knocked RPM (RPMN), *Nf1*-and *Pten*-knocked RPM (RPMNP), and p62-knocked RPMNP (RPMNP-p62KO) cells were established via lentiviral infection. The CRISPR Oligo and in-fusion sequences used were as follows:

Pten CRISPR Oligo1 CACCGAGATCGTTAGCAGAAACAAA.
Pten CRISPR Oligo2 AAACTTTGTTTCTGCTAACGATCTC.
Nf1 CRISPR Oligo1 CACCGCTCGTCGAAGCGGCTGACCA.
Nf1 CRISPR Oligo2 AAACTGGTCAGCCGCTTCGACGAGC.
Sqstm1 CRISPR Oligo1 CACCGATGGTGGGCGATGTTCCCGC.
Sqstm1 CRISPR Oligo2 AAACGCGGGAACATCGCCCACCATC.
Blasticidin resistance gene Forward GAGAATCCTGGACCGACCATG AAAACATTTAACATTTC.
Blasticidin resistance gene Reverse GTCGACTTAACGCGTTTATT TCGGGTATATTTGAGTG.
Zeocin resistance gene Forward GAGAATCCTGGACCGATGGCCAA GTTGACCAGTG.
Zeocin resistance gene Reverse GTCGACTTAACGCGTTCAGTCCTG CTCCTCGGC.
CRISPR V2 Forward ACGCGTTAAGTCGACAATCAACCTCTGGAT.
CRISPR V2 Reverse CGGTCCAGGATTCTCTTCGACATCTCCGGC.

For single-organoid cloning to establish RPM, RPMN, RPMP, and RPMNP organoids, the organoids were trypsinized and dissociated. The dissociated cells were diluted with the medium, mixed with Matrigel, and covered with the organoid medium containing 10 μM Y-27632. After 7–14 days, the clonal organoids were picked, expanded, and screened for mutations in the target genes. Clonally expanded cell lines were confirmed using Sanger DNA sequencing and whole exome sequencing (WES). For Sanger sequencing, genomic DNA was extracted from the cells using the DNeasy Blood & Tissue Kit (Qiagen) according to the manufacturer's instructions. Subsequently, the deleted DNA regions were PCR-amplified using primers spanning the potential deletion sites with Prime STAR GXL Premix (Takara). After separation on an agarose gel, the DNA fragments were excised and purified using the QIAquick Gel Extraction Kit (Qiagen) following the manufacturer's instructions. Subsequently, the DNA fragments were PCR-amplified using the In-Fusion primers. After separation on an agarose gel, the DNA fragments were excised and purified. The DNA fragments were cloned into BamHI-digested pUC19 (RRID: Addgene_50005) using In-Fusion (Takara). The transformation products using DH5α were spread on LB Agar Carbenicillin plates and incubated overnight at 37 °C. Colonies were sequenced using FASMAC, and the data were analyzed. The sequences used were as follows:

In-Fusion pUC-*Trp53*KO Forward CGACTCTAGAGGATCCTGTGC AGTTGTGGGTCA.
In-Fusion pUC-*Trp53*KO Reverse CGGTACCCGGGGATCATCACCAT CGGAGCAGCG.
Trp53 sequence primer CTGTGCAGTTGTGGGTCAGC & ATCACC ATCGGAGCAGCG.

2.6. qPCR

Total RNA was isolated from organoids or 2D cultured cells using an RNeasy Mini Kit (Qiagen), followed by the removal of genomic DNA and reverse transcription using the PrimeScript RT Reagent Kit with gDNA Eraser (Perfect Real Time) (Takara), in principle. Reverse transcription (RT)-qPCR was performed using a StepOnePlus Real-Time PCR System (Applied Biosystems), Thermal Cycler Dice Real Time System TP800 (Takara), or CFX Duet Real-Time PCR System (Bio-Rad). The primer sequences used were as follows:

Trp53 Forward GCGTAAACGCTTCGAGATGTT.
Trp53 Reverse TTTTTATGGCGGGAAGTAGACTG.
Myc Forward CCTAGTGCTGCATGAGGAGA.
Myc Reverse TCTTCCTCATCTTCTTGCTCTTC.
Rb1 Forward TGCATCTTTATCGCAGCAGTT.
Rb1 Reverse GTTCACACGTCCGTTCTAATTTG.
Sqstm1 Forward AGGATGGGGACTTGGTTGC.
Sqstm1 Reverse TCACAGATCACATTGGGGTGC.
Ho-1 Forward AAGCCGAGAATGCTGAGTTCA.
Ho-1 Reverse GCCGTGTAGATATGGTACAAGGA.
Nqo1 Forward AGGATGGGAGGTACTCGAATC.
Nqo1 Reverse AGGCGTCCTTCCTTATATGCTA.
Lamp1 Forward CAGCACTCTTTGAGGTGAAAAAC.
Lamp1 Reverse ACGATCTGAGAACCATTCGCA.
Rubcn Forward CAGGGTGTAGTGCATGGTTCT.
Rubcn Reverse CCGCCAAGATCCATTCCCG.
Vcp Forward CGACCCAATCGGTTAATTGTTGA.
Vcp Reverse AGCTTCCCGTCTTTTCTTTCC.
Actb Forward GGCATAGAGGTCTTTACGGATGTC.
Actb Reverse TATTGGCAACGAGCGGTTCC.

2.7. Western blotting

Cell pellets were lysed in 2 × sodium dodecyl sulfate buffer or RIPA lysis buffer containing 0.1 M dithiothreitol and the protease inhibitor cOmplete MINI. The protein concentrations were determined using the Pierce BCA protein assay kit (Thermo Fisher Scientific). Approximately equal amounts of protein extracts were loaded and separated by sodium dodecyl sulfate-polyacrylamide gel electrophoresis and transferred onto a PVDF membrane (Millipore IPFL00010). The membranes were blocked at room temperature with 5 % non-fat milk in TBS plus 0.05 % Tween 20 (TBS-T), followed by incubation with primary antibodies. The blots were washed and incubated with fluorescent-labeled anti-mouse IgG or anti-rabbit IgG at room temperature. The membranes were analyzed by enhanced chemiluminescence (PerkinElmer) using LAS-3000 (FujiFilm). Information regarding the antibodies is shown in Supplementary Table 4.

2.8. Drug sensitivity assays

The tumor cells harvested using TrypLE were filtered using a 100-μm nylon cell strainer and counted using Trypan blue with a cell counter. The cells were seeded in 96-well plates on day 1. The indicated concentrations of CBDCA, PTX, olaparib, everolimus, combinations of drugs, or vehicle were added when refreshing the culture medium on day 2. ATP levels were measured using CellTiter-Glo 2.0 (Promega) according to the manufacturer's instructions, and luminescence was measured on day 5 using an EnVision multimode plate reader (PerkinElmer), in principle. The results were normalized to those of the control samples and analyzed. An extra sum-of-squares F test was used to analyze the differences in the IC50 of each compound.

2.9. Cell lines and cell cultures

All cell lines were cultured under 5 % CO_2 at 37 °C. The human ovarian cancer cell line Caov3 was cultured in culture medium (D-MEM/Ham's F-12 with L-glutamine and phenol red [Wako] supplemented with approximately 10 % fetal bovine serum). SKOV3 was cultured in RPMI Medium 1640 (Gibco) supplemented with 10 % fetal bovine serum. After establishing HGSC-modeling organoids from nFTE organoids, each organoid was cultured in culture medium (D-MEM/Ham's F-12 with L-glutamine and phenol red [Wako] supplemented with approximately 10 % fetal bovine serum) as a cell line. All the cell lines tested negative for mycoplasma contamination.

2.10. Colony formation assays

The tumor cells harvested using TrypLE were filtered using a 100-μm nylon cell strainer and counted using Trypan blue with a cell counter or hemocytometer (Burker-Turk board). cRPM-EGFP, RPMNP, cRPM-p62OE, RPMNP-p62KO, Caov3 cells, and SKOV3 cells were seeded into 6 well plates on day 1. The indicated concentrations of CBDCA, PTX, everolimus, combinations of drugs, or vehicle were added for 6 days. The total number of culture days and primary numbers of seeded cells were optimized for each cell line. On the final day, after the wells were washed with cold PBS, the cells were fixed with cold methanol. The cells were stained with crystal violet solution and washed with water. After drying at room temperature overnight, the stained cells were scanned with backing white paper and analyzed using "ImageJ" software. The sum-of-squares F test or Student's *t*-test was used to evaluate the efficacy of each compound.

2.11. RNA sequence analysis

Cultured organoids were processed for RNA extraction using an RNeasy Plus Mini Kit (Qiagen) according to the manufacturer's instructions. The NEBNext Ultra II Directional RNA Library Prep Kit (New England Biolabs) was used to prepare the sequencing libraries. All libraries were assessed using a TapeStation4200 (Agilent) and quantified using Qubit4.0 (Thermo Fisher Scientific). Multiplexed library pools were sequenced using 50 bp PE reads on a NextSeq2000 platform (Illumina). The sequencing reads from FASTQ files were trimmed and mapped to the reference mouse genome "GRCm39", and read counts were obtained using CLC Genomics Workbench (Qiagen). Heatmap analysis was performed using TPM values. The distance measure was based on the Euclidean distance, and the linkage criterion was complete linkage. We used pre-ranked gene set enrichment analysis to compare gene expression based on $\log_2$ (normalized TPM ratio) of genes, except for those with extremely low expression.

2.12. DIA proteomic analysis

The proteins in the cell samples were extracted in 100 mM Tris-HCl (pH 8.5) containing 2 % sodium dodecyl sulfate (SDS) using a sonicator. The protein extracts were reduced with 20 mM TCEP (tris(2-carboxyethyl)phosphine) at 80 °C and alkylated using 35 mM iodoacetamide at room temperature. Proteins were purified and digested using the sample preparation (SP3) method. Tryptic digestion was performed using 500 ng of Trypsin/Lys-C Mix (Promega) overnight at 37 °C. The cell digests were purified using a GL-Tip SDB (GL Sciences) according to the manufacturer's protocol. The peptides were dissolved again in 2 % acetonitrile (ACN) containing 0.1 % trifluoroacetic acid (TFA) and then quantified for LC-MS analysis. Two mobile phases, A and B, containing H_2O and 80 % ACN/H_2O (4/1 v/v) were prepared in 0.1 % formic acid (FA). Subsequently, 300 ng of the digested peptides were loaded onto an UltiMate 3000 RSLC nano system (Thermo Fisher Scientific). The eluted peptides were analyzed using Q Exactive HF-X (Thermo Fisher Scientific) for overlapping window DIA. The LC-MS/MS data were analyzed using Scaffold DIA (Proteome Software) with mouse spectral libraries built from the mouse UniProtKB/Swiss-Prot database. Peptides and proteins whose FDR values were 1 % or less were identified and quantified. In addition, we analyzed the expression values after grouping relative proteins, normalizing them to the median, and excluding proteins with one unique peptide or with no expression in one or more samples. To explore significant factors related to mTOR signaling, we listed and analyzed proteins related to "mouse-ortholog hallmark mTORC1 signaling".

2.13. Exome sequencing and data analysis of mouse organoids

DNA was isolated from the cultured organoids using the QIAamp DNA Mini Kit (Qiagen) according to the manufacturer's instructions. The DNA purity and concentration were examined using a NanoDrop2000 spectrophotometer. The genomic DNA samples were fragmented using a sonicator. The fragments were treated with End Prep Enzyme Mix for end repair, and their sizes were selected. Poly-A tails were added to the 3′ ends using A Tailing Mix and then purified. The adaptors were ligated at both ends of the purified protein. After size selection, the products were amplified using Pre-Capture PCR primers. To capture exon regions, the Block Mix, Hybridization Buffer, and Capture Library were poured into a 750 ng library for 24 h. Dynabeads MyOne Streptavidin T1 magnetic beads were used to elute the capture products. Each sample was then amplified using the PCR primers P5 and P7. After library preparation, the size and concentration of each sample were determined. Each captured library was then loaded onto an Illumina NovaSeq for 2 × 150 paired-end sequencing, according to the manufacturer's instructions (Illumina). Raw image files and base calling were conducted using the NovaSeq Control Software (NCS) + OLB + GAPipeline-1.6 (Illumina) on the NovaSeq instrument. After removing the adaptor reads using Cutadapt, the clean data were aligned with the reference genome using BWA (RRID:SCR_010910), and duplications were removed using Picard (RRID:SCR_006525). GATK (RRID:SCR_001876) or SAMtools (RRID:SCR_00210) was used to call SNVs/InDels, and the variants were annotated using ANNOVAR (RRID:SCR_012821). Somatic variation analysis was performed using Mutect2 when necessary.

2.14. Autophagy assay using flow cytometry

RPM and RPMNP cells stably expressing GFP-LC3B-mRuby3-LC3ΔG were cultured in fetal bovine serum-supplemented culture medium for approximately 16 h. After the cell culture dishes were adequately washed with PBS, the cells were starved in serum- and amino acid-free culture medium (DMEM [high glucose] with sodium pyruvate without amino acids; Wako). After the starved cells were harvested with TrypLE at certain time points, the cells were suspended in PBS and analyzed with an Attune Acoustic Focusing Cytometer (Thermo Fisher Scientific). Flow cytometry data analysis was performed using the software "FlowJo" (Becton Dickinson). The cells harvested without starvation were used as controls, and the GFP- and mRuby3-negative controls were the cells that did not express GFP-LC3B-mRuby3-LC3ΔG.

2.15. Human samples

Patient data and ovarian cancer tissue samples were collected at the University Hospital with the approval of the Institutional Ethics Committee (Approval Nos. 20070081 and 20210111). This study was performed in accordance with the relevant guidelines and regulations. All participants were females. Patient information, including age and stage, is shown in Table 1. They were informed of the study and provided informed consent to participate. HGSC-resected tumor samples were fixed in formalin and paraffin embedded (FFPE).

Table 1
Clinical profiles of 15 pairs of high-grade serous carcinoma samples. Age: at an interval debulking surgery (IDS). Progression-free survival: elapsed days from last platinum treatment to progression or the last follow-up day (the day of computed tomography or CA125 monitoring by blood test). A refractory case is indicated in red letters. *BRCA1/2* status: the pathogenic mutation profile of genome (g) or tumor (t) *BRCA1/2* from the most reliable medical resources at that time (+: pathogenic mutation-positive; -: pathogenic mutation-negative). HRD status: the level of homologous recombination (HR) deficiency determined by the *BRCA1/2* status and genome instability score (if the score is equal to or less than 42, HRD positive). In the regimen, TC: carboplatin + paclitaxel, BEV: bevacizumab, OLA: olaparib, PLD: doxorubicin; maintenance therapy indicated chemotherapy after IDS until progression. Progression: + indicated recurrence confirmed by computed tomography in principle.

Case No.	Histology	Age	Stage	PFS	*BRCA1/2* status	HRD status	Regimen			Surgery	progression
							Neoadjuvant chemotherapy	Chemotherapy post surgery	Maintenance therapy		
pSOC-1	HGSC	58	IIIC	1018*	t (−)	+	TC, BEV	TC, BEV	BEV, OLA	complete	−
pSOC-2	HGSC	75	IIIC	415	t (−)	−	TC, BEV	TC, BEV	BEV	complete	+
pSOC-3	HGSC	68	IIIC	673*	t (+) g (−)	+	TC, BEV	TC	OLA	complete	−
pSOC-4	HGSC	71	IVB	Ref	t (−)	−	TC, BEV	TC	−	optimal	+
pSOC-5	HGSC	60	IVB	322	t (−)	+	TC, BEV	TC	OLA	optimal	+
pSOC-6	HGSC	77	IVB	609*	t (+) g (+)	+	TC	TC, BEV	BEV, OLA	complete	−
pSOC-7	HGSC	41	IIIC	305	t (−)	+	TC	TC	Niraparib	complete	+
pSOC-8	HGSC	60	IIIA1 (ii)	15	t (−)	−	TC	TC	−	complete	+
pSOC-9	HGSC	49	IIIC	535	g(−)	NA	TC, BEV	TC, BEV	BEV	complete	+
pSOC-10	HGSC	62	IIIC	333	g(−)	NA	TC, BEV	TC, BEV	BEV	complete	+
pSOC-11	HGSC	75	IVB	250*	t (+)	+	TC	TC	Niraparib	optimal	−
pSOC-12	HGSC	73	IIIC	464	t (+) g (+)	+	TC	TC	Niraparib	optimal	+
pSOC-13	HGSC	44	IVB	296*	t (−)	+	TC	TC, BEV	BEV	complete	−
pSOC-14	HGSC	46	IIIC	496	t (−)	−	TC, BEV	TC, BEV	BEV	complete	+
pSOC-15	HGSC	76	IIIC	191	t (−)	−	TC	TC	Niraparib	optimal	+

PFS: Progression free survival (Day 0: Last platinum treatment), *No progression , HRD = {*BRCA1/2* pathogenic variant(+) or GIS ≥ 42}

2.16. Immunohistochemistry (IHC), immunofluorescence (IF), and multiplex IF

For IHC and IF, organoids in Matrigel were collected from culture plates, fixed with formalin, and embedded in paraffin. FFPE specimen slides were deparaffinized using Clear Plus (or xylene) and ethanol. Hematoxylin and eosin staining, IHC, IF, and multiplex IF were performed. Information regarding the antibodies used and the optimized procedures used for each protein is shown in Supplementary Table 4. For multiplex IF, each protein was stained as follows:

We activated the antigens with AR6 or AR9 buffer diluted in water at 95 °C or 120 °C for the optimized time and placed the slides in TBS-T after quenching. The membrane was blocked with a primary antibody diluted in an antibody diluent/block at room temperature. The slides were washed with TBS-T, and Opal Polymer HRP MS + Rb was added to the slides at room temperature. After washing with TBS-T, each color Opal Fluorophore in a 1 × Plus Amplification Diluent was added to the slides for 10 min at room temperature. Finally, the specimens were stained with Spectral DAPI at room temperature and washed. The slides were scanned using Vectra Polaris, and image quantification analysis was performed with the software "inForm."

2.17. Statistical analysis

Statistical analyses and computational analyses were performed using the GraphPad Prism software, R, or Python (RRID:SCR_024202).

2.18. Data availability

The RNA-sequencing data have been deposited in the Gene Expression Omnibus (GEO) (RRID:SCR_005012) with GEO accessions GSE255127 and GSE255128.

3. Results

3.1. Aberrant RAS/PI3K signaling activation as a prominent signature of poor prognosis in patients with BRCA1/2 WT ovarian cancer

To explore the critical biological processes that determine prognosis in patients with advanced HGSC, we performed a gene set variation analysis (GSVA) in 391 patients with advanced serous ovarian cancer (WHOLE) from the TCGA ovarian cancer dataset and investigated the relationship between prognosis and activation of pathways related to biological processes (Fig. S1A). GSVA is a method used to score the activity of certain pathways in each sample; we used it to allocate patients with ovarian cancer into two groups according to the scores of all pathways [11] (Fig. 1a). As a result, the activation of 23 pathways among the 1590 pathways significantly correlated with the prognosis in WHOLE patients ($p < 0.01$); the activation of pathways such as "sterol transport" and "inorganic anion transport" prominently correlated with poor prognosis (Fig. 1b, Supplementary Table 1). Of note, recent studies have reported that the membrane transportation of cholesterol induces tumor-associated macrophages to undergo reprogramming and drives tumor growth and that SLC34A2-XPR1-mediated phosphate homeostasis is critical for the survival of ovarian cancer cells, which supports the validity of this computational method for discovering key pathways determining prognosis in patients with serous ovarian cancer [12,13].

To identify essential biological pathways that uniquely determine prognosis in patients with advanced *BRCA1/2* WT HGSC, we performed GSVA in 202 patients with advanced *BRCA1/2* WT serous ovarian cancer (BRCA-WT) from the TCGA ovarian cancer dataset and investigated the relationship between prognosis in BRCA-WT patients and the activation of each pathway in the same way. Consequently, the activation of GTPase-related pathways such as "regulation of small GTPase-mediated signal transduction" was identified as the most prominent poor prognostic factor in BRCA-WT patients rather than in WHOLE patients (Fig. 1c, Supplementary Table 2). Notably, in GTPase-family

signal transduction pathways, the activation of "RAS protein signal transduction" correlated with poor prognosis in BRCA-WT patients (Fig. 1d). Consequently, to visualize the coordination of significant pathways in BRCA-WT patients ($p < 0.05$), we grouped the significant pathways using the variational Bayesian Gaussian mixture model by GSVA score, which showed that only seven pathways corresponded to GTPase-related pathways, including inositol lipid metabolism pathways such as "phosphatidylinositol 3 kinase signaling" (Fig. 1e, Fig. S1B and

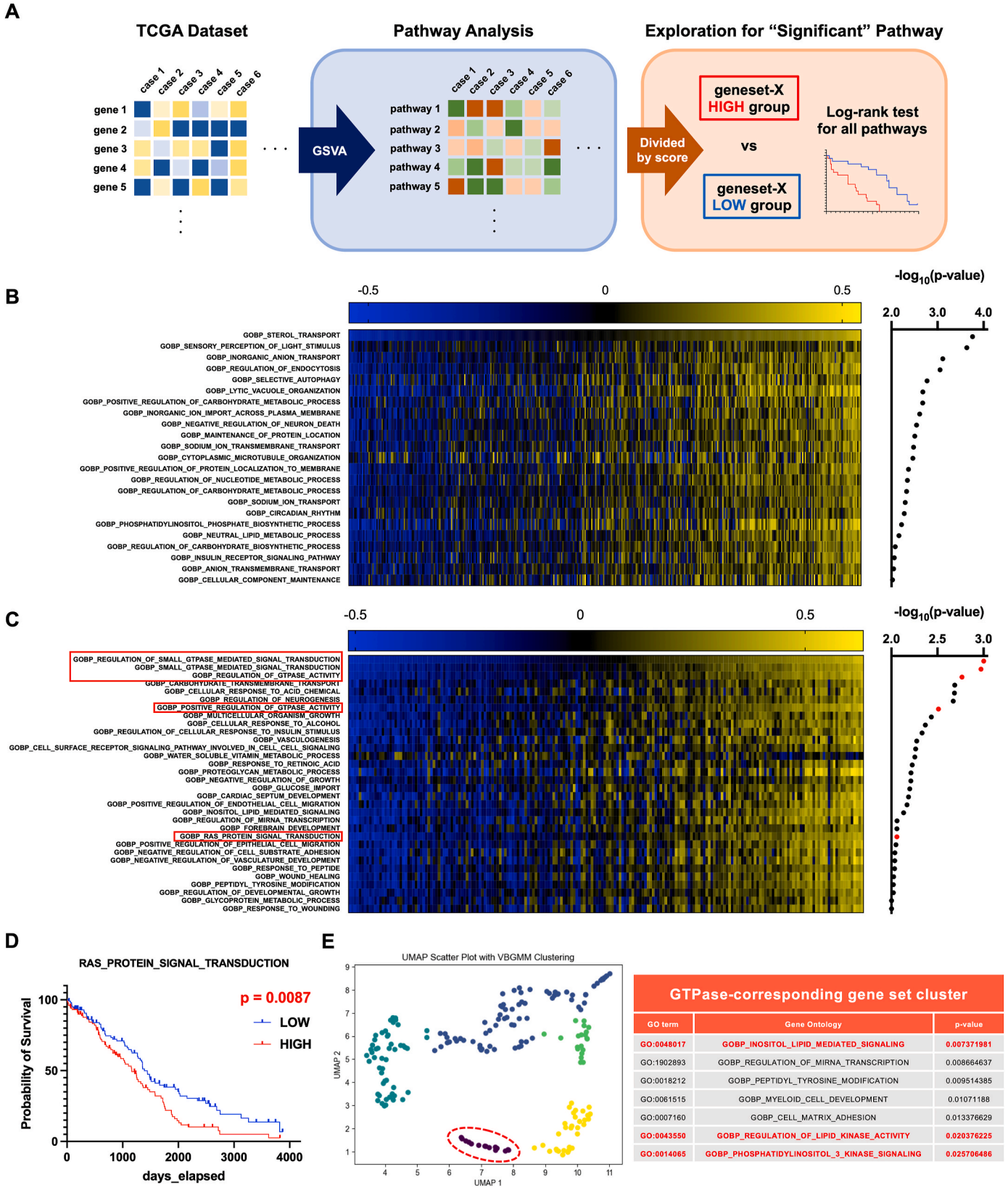

(caption on next page)

Fig. 1. Computational approaches revealed new pathways strongly associated with progression in TCGA advanced ovarian cancer cases.
A, Schematic representation of the computational approach using an R package "GSVA" (gene set variation analysis) and transcriptomic data sets of TCGA advanced ovarian cancer cases; **B**, Heatmap depicted by GSVA scores of pathways with $p < 0.01$ in biological process ontology, ranked by log-scale p-values from log-rank tests which examined the correlation between GSVA scores and prognosis in whole advanced ovarian cancer patients ($n = 391$). Each column indicates GSVA score of one case. Cases were ordered according to the GSVA scores of the most significant pathway "sterol transport"; **C**, Heatmap depicted by GSVA scores of pathways with $p < 0.05$ (only pathways with $p < 0.01$ were listed) in biological process ontology, ranked by log-scale p-values from log-rank tests which examined the correlation between the GSVA score and prognosis in *BRCA1*/2-WT advanced ovarian cancer patients ($n = 202$) rather than in whole advanced ovarian cancer patients ($n = 391$). Each column indicates GSVA score of one case. Cases were ordered according to the GSVA scores of the most significant pathway "regulation of small GTPase mediated signal transduction". The pathways emphasized by red boxes are related to GTPase activity; **D**, Kaplan–Meier survival curves depicted according to RAS-relating signaling transduction score (RAS-score) calculated using the GSVA score and prognosis of *BRCA1*/2-WT advanced ovarian cancer patients (a blue line including patients with RAS-score less than 0; a red line including patients with RAS-score more than or equal to 0). Log-rank test; **E**, UMAP scatter plot using GSVA scores of significant pathways ($p < 0.05$) in *BRCA1*/2-WT advanced ovarian cancer patients rather than in whole advanced ovarian cancer patients. Variational Bayesian Gaussian Mixture Model (VBGMM) was used for gene set clustering, and the cluster including "regulation of small GTPase mediated signal transduction" was named and listed as "GTPase-corresponding gene set cluster". (For interpretation of the references to color in this figure legend, the reader is referred to the Web version of this article.)

C). Clustering analysis suggested that the activation of phosphatidylinositol 3 kinase (PI3K) signaling corresponded to that of RAS signaling and that aberrant RAS/PI3K pathways could contribute to poor progression in patients with *BRCA1/2* WT ovarian cancer. As a supplement, we also investigated the relationships between the activation of the RAS and PI3K pathways and prognosis in patients with *BRCA1/2*-mutated advanced serous ovarian cancer (BRCA-MU), which showed that the activation of either the RAS or the PI3K pathway did not affect the prognosis of BRCA-MU patients (Fig. S1D and E).

As previously reported by the TCGA research network, copy number alterations and gene expression changes that upregulate the RAS/PI3K pathway are common events in patients with HGSC [8]. In BRCA-WT patients, driver mutations in *KRAS* and *PIK3CA* were rarely detected, whereas copy number alterations in *KRAS*, *PIK3CA*, *NF1*, and *PTEN* were frequently detected (Fig. S1F and G). We assumed that the aberrant RAS/PI3K signaling activation triggered by these copy number alterations was a poor prognostic signature in patients with *BRCA1/2* WT HGSC and utilized our newly established experimental models for the pursuit of background mechanisms.

3.2. Generation of organoid model mimicking human HGSC derived from murine fallopian tubes

After confirming that the murine fallopian tube epithelium comprised secretory and ciliated cells, similar to the human fallopian tube epithelium [14] (Fig. 2a, Fig. S2A), we established a normal fallopian tube epithelium organoid (cas-nFTE) from a *B6J.129(B6N)-Gt(ROSA)26Sor*$^{tm1(CAG\text{-}cas9^{*}\text{-}EGFP)Fezh}$*/J* mouse [15]. We knocked out *Trp53* by introducing sgRNA into cas-nFTE organoids, nutlin selection, and single-organoid cloning. The *Trp53*-knockout cas-nFTE organoids (casP) grew faster than did the cas-nFTE organoids (Fig. 2b, Fig. S2B). After confirming clonality by whole exome sequencing (WES), we analyzed the transcriptomic differences caused by *Trp53* knockout by RNA sequencing and gene set enrichment analysis (GSEA) [16], which indicated that casP organoids exhibited reduced expression of cilium-related gene sets (Fig. 2c, Fig. S2C). In human HGSC precancerous lesions, such as serous tubal intraepithelial carcinoma (STIC), differentiation into ciliated cells has been reported to be down-regulated [17]; therefore, genetic manipulation to cas-nFTE is thought to mimic the process of carcinogenesis of HGSC. Consequently, we evaluated the tumorigenesis of casP in vivo by transplanting casP cells into nude mice subcutaneously; however, casP cells could not develop any subcutaneous tumor mass, suggesting that inactivation of the p53 pathway is not sufficient for oncogenic transformation of the fallopian tube epithelium.

Since frequent genetic alterations related to *TP53*, *RB1*, and *MYC* in HGSC have been reported in TCGA studies, we adopted a normal fallopian tube epithelium organoid (nFTE) established from an *Rb1*$^{fl/fl}$*Trp53*$^{fl/fl}$*Myc*$^{LSL/LSL}$ mouse as the source for the HGSC organoid model [8,18] (Fig. 2d). After confirming that nFTE organoids were composed of secretory and ciliated cells (Fig. S2D), *Rb1* and *Trp53* were knocked out, and *Myc* was overexpressed in nFTE organoids by introducing *Cre* (mFTE and cRPM). The genetic manipulation used to generate mFTE organoids resulted in depletion of *Rb1* and *Trp53* and overexpression (OE) of *Myc* at the RNA level and an increase in MKI67-expressing cells (Fig. 2e, Fig. S2E). Moreover, mFTE organoids were able to develop subcutaneous tumors well-stained with human HGSC marker proteins, such as PAX8 and WT1 in nude mice (Fig. 2f). As the subcutaneous tumor mimicked human HGSC pathology characterized by papillary morphology and high nuclear grade, an *Rb1*$^{-/-}$*Trp53*$^{-/-}$*Myc*^{OE} HGSC-modeling organoid (RPM) was established from the subcutaneous tumor. Thus, to investigate how the aberrant RAS/PI3K pathway affects the phenotypes of *BRCA1/2* WT HGSC, we generated HGSC-modeling organoids with different genetic alterations from the RPM organoid by stepwise genetic engineering. We knocked out *Nf1*, *Pten,* or both of them from the RPM organoid using the CRISPR/Cas9 system and successfully generated various HGSC-modeling organoids (*Rb1*$^{-/-}$*Trp53*$^{-/-}$*Myc*^{OE} with *Nf1* knocked: RPMN; *Rb1*$^{-/-}$*Trp53*$^{-/-}$*Myc*^{OE} with *Pten* knocked: RPMP; and *Rb1*$^{-/-}$*Trp53*$^{-/-}$*Myc*^{OE} with *Nf1* and *Pten* knocked: RPMNP) (Fig. 2g). The activation of the RAS and PI3K pathways and the clonality of all the established organoids were confirmed using western blotting (WB) and WES, respectively (Fig. 2h, Fig. S2F). We also performed RNA sequencing and unsupervised hierarchical clustering based on the transcriptomic profiles of the nFTE, RPM, RPMN, RPMP, and RPMNP organoids, which indicated that the four HGSC-modeling organoids were transcriptionally distant from the nFTE organoid (Fig. 2I).

3.3. Aberrant RAS/PI3K signaling activation deteriorates prognosis and hampers autophagy

To characterize our HGSC models in vivo, we inoculated RPM, RPMN, RPMP, and RPMNP cells intraperitoneally and compared the survival of the recipient mice. All cells formed a tumor mass, and the mice that received RPMNP cells had the worst survival (Fig. 3a). Consistent with in vivo growth, in vitro growth was accelerated by aberrant RAS/PI3K pathway activity in RPMNP cells (Fig. 3b). Chemosensitivity tests showed that RPMN cells were more resistant to CBDCA and PTX, and that RPMP cells were more resistant to CBDCA compared with RPM cells. Notably, RPMNP cells showed robust resistance to CBDCA, PTX, and olaparib (Fig. 3c–e), suggesting that aberrant RAS/PI3K pathway activity caused by *Nf1* or *Pten* loss contributes to the poor progression of *BRCA1/2* WT HGSC, which is consistent with the results of our computational analysis.

To investigate the transcriptomic changes following genetic manipulation in the organoid lines, we performed GSEA on mSigDB hallmark gene sets between the RPM and RPMNP organoids. The analysis showed that, in the RPMNP organoids, cell growth-related gene sets such as "MYC targets v1/2," "E2F targets," and "G2M checkpoint" were activated, and the gene set "apoptosis" was suppressed, which supported the transcriptomic features of the poor progression of the RPMNP cells (Fig. 3f).

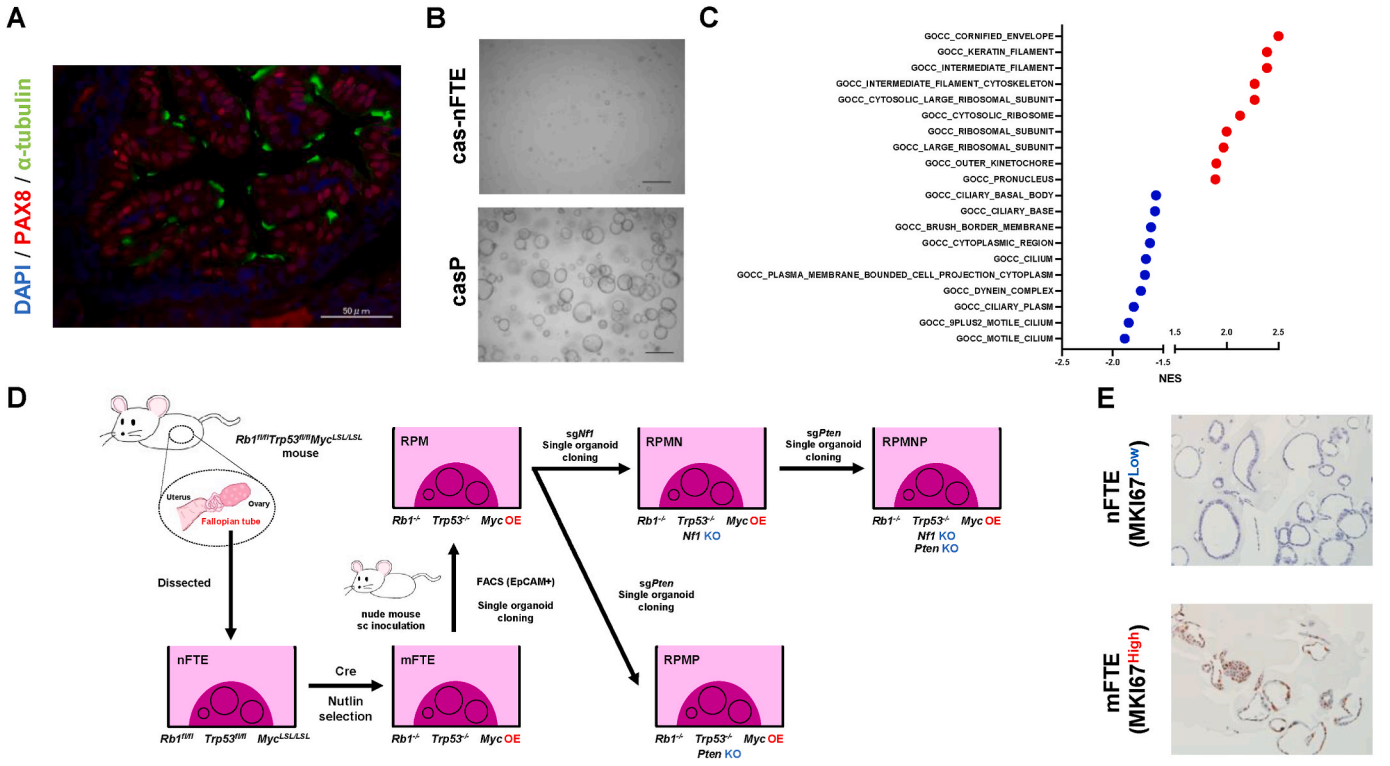

(caption on next page)

Fig. 2. Generation of organoid model mimicking human HGSC derived from murine fallopian tubes.
A, Immunofluorescence of normal fallopian tube epithelium dissected from a nude mouse stained with PAX8 (red), α-tubulin (green), and DAPI (blue). Scale-bar indicated 50 μm; **B**, Brightfield image of organoids established from *B6J.129(B6N)-Gt(ROSA)26Sor*$^{tm1(CAG-cas9*,-EGFP)Fezh}$/J mice. cas-nFTE: normal fallopian tube epithelium organoids. casP: *Trp53*-knocked out cas-nFTE organoids. Scale-bars indicated 500 μm; **C**, RNA-sequencing analysis by pre-ranked Gene Set Enrichment Analysis (GSEA) indicating enrichment of mSigDB gene ontologies in cellular component in casP organoids compared with cas-nFTE organoids. The y-axis represents gene sets, and the x-axis represents normalized enrichment score (NES); **D**, Schematic representations of the procedure of murine HGSC-modeling organoid establishment from an *Rb1*$^{fl/fl}$*Trp53*$^{fl/fl}$*Myc*$^{LSL/LSL}$ mouse; **E**, Representative immunohistochemistry image of nFTE organoids and mFTE organoids stained with MKI67; **F**, *In vivo* imaging of mFTE-derived subcutaneous tumor taken on day 13 by intravenous injection of luciferin. H&E stain and IHC of mFTE-derived subcutaneous tumors harvested on day 50 stained with WT1, PAX8, MYC, and MKI67; **G**, Representative brightfield image of the organoid spheres (RPM: *Rb1*$^{-/-}$*Trp53*$^{-/-}$*Myc*^{OE}, RPMN: *Rb1*$^{-/-}$*Trp53*$^{-/-}$*Myc*^{OE} + *Nf1*KO, RPMP: *Rb1*$^{-/-}$*Trp53*$^{-/-}$*Myc*^{OE} + *Pten*KO, RPMNP: *Rb1*$^{-/-}$*Trp53*$^{-/-}$*Myc*^{OE} + *Nf1*KO + *Pten*KO). Normal fallopian tube epithelium (nFTE) organoids were established from an oviduct of an *Rb1*$^{fl/fl}$*Trp53*$^{fl/fl}$*Myc*$^{LSL/LSL}$ mouse. Scale-bar indicated 100 μm; **H**, Western blotting of RPM, RPMN, RPMP, and RPMNP cells. GAPDH, NF1, PTEN, MEK, pMEK, AKT, and pAKT(Ser473); **i**, Unsupervised hierarchical clustering of RNA-seq expression data from nFTE (RPM_normal), RPM, RPMN, RPMP, RPMNP organoids. The below color bar indicated corresponding z-score to each color. (For interpretation of the references to color in this figure legend, the reader is referred to the Web version of this article.)

Importantly, the analysis indicated simultaneous activation of the "mTORC1 signaling" and "unfolded protein response" pathways, which are known to inversely regulate autophagy, in the RPMNP organoids (Fig. S3A and B) [19]. GSEA between RPM and RPMNP organoids regarding a gene set "autophagosome maturation" showed that the early phase of autophagy was significantly downregulated in the RPMNP organoids (Fig. 3g); therefore, we assumed that aberrant RAS/PI3K signaling activation inhibits autophagy in the RPMNP organoids. We validated some genes in "autophagosome maturation" using qPCR (Fig. S3C). To visualize autophagy flux in vitro, we generated RPM and RPMNP cells stably expressing a fluorescent probe to evaluate autophagic flux, GFP-LC3-mRuby3-LC3ΔG, and analyzed autophagy flux under starvation conditions by the relative fluorescence intensity of GFP to that of mRuby3 (Fig. S3D) [20]. Flow cytometry showed that GFP-LC3 was well retained in RPMNP cells compared with that in RPM cells during starvation, and the mTOR inhibitor everolimus (EVL) induced the degradation of GFP-LC3 in RPMNP cells (Fig. 3h–j). These findings suggest that autophagy flux is hampered by aberrant RAS/PI3K pathways that lead to mTOR signaling activation in RPMNP cells and that pharmacological inhibition of mTOR results in the induction of autophagy.

3.4. Autophagic degradation of p62 is attenuated by mTOR, leading to platinum resistance

To examine whether the activation of mTOR signaling could influence HGSC tumor progression, we evaluated the effects of EVL on the proliferation of RPM, RPMN, RPMP, and RPMNP cells. The proliferation of RPM, RPMN, and RPMP cells was inhibited to some extent by EVL treatment; however, the proliferation of RPMNP cells, the HGSC model in which mTOR signaling was activated, was not affected (Fig. S4A and B). To evaluate the influence of mTOR signaling on chemosensitivity, we treated RPMNP cells with CBDCA and EVL; as a result, EVL enhanced the antitumor efficacy of CBDCA in RPMNP cells (Fig. 4a). In addition, the combined effect of EVL against the human *BRCA1/2* WT ovarian cancer cell line Caov3 and SKOV3 was shown (Fig. 4b) [21].

To investigate the molecular mechanism of the combined effect, we performed proteomic exploration in RPM, RPMNP, and EVL-treated RPMNP cells regarding proteins included in a gene set "mTORC1 signaling" (Supplementary Table 3). Consequently, p62 (SQSTM1) was detected as a potential protein whose expression was increased by aberrant RAS/PI3K signaling activation and decreased by EVL-induced pharmacological inhibition of mTOR (Fig. 4c and d). Immunoblot analysis revealed that the abundance of the p62 protein and the phosphorylation status of the S6 protein, a marker of mTOR signaling activation, were greater in the RPMN, RPMP, and RPMNP cells than in the RPM cells (Fig. 4e). These findings suggest that genetic manipulation to activate RAS or PI3K signaling leads to an increase in the abundance of p62 protein through mTOR signaling activation.

To investigate the effects of p62 expression on chemosensitivity, we generated RPMNP cells with p62 knocked down (RPMNP-p62KO) and cRPM cells overexpressing p62 (cRPM-p62OE) (Fig. S4C). Chemosensitivity tests revealed that, compared with RPMNP cells, RPMNP-p62KO cells were more sensitive to CBDCA and TC treatments (CBDCA + PTX), the standard treatment in patients with HGSC (Fig. 4f, Fig. S4D). In addition, cRPM-p62OE cells were more resistant to CBDCA than cRPM cells expressing EGFP (Fig. 4g). Next, we investigated the regulation of p62 expression in HGSC; p62 is known to function as a ubiquitin-binding protein that induces the aggregation of unnecessary proteins and is degraded during autophagy. Thus, we quantified the level of intracellular p62 when EVL alone or EVL along with hydroxychloroquine, an autophagy inhibitor, were added. The degradation of p62 by EVL was recovered by inhibiting autophagy; autophagy inhibition slightly activated mTOR signaling (Fig. 4h). These results suggest that EVL enhances the efficacy of platinum-based chemotherapy in refractory *BRCA1/2* WT HGSC by promoting the autophagic degradation of p62.

3.5. p62-mediated NRF2 antioxidant pathway activation driven by RAS/PI3K-mTOR triggers poor PFS in ovarian cancer

To investigate the mTOR-p62 pathway in a patient with refractory HGSC, we performed multiplex immunofluorescence analysis of tumor samples from patients with refractory *BRCA1/2* WT HGSC. We found that p62 and phospho-S6 (pS6) colocalized in CK-positive tumor regions, which supported our findings in murine HGSC models (Fig. 5a, Fig. S5A).

Next, we investigated the ability of p62 to reduce the toxicity of platinum-based chemotherapy. p62 has been reported to possess several domains that trigger the activation of several pathways, such as the NRF2 signaling pathway [22]. We previously reported that high expression of p62 was associated with poor prognosis in patients with ovarian cancer [23]; however, the role of p62 in the chemoresistance of HGSC has not been determined. To investigate how p62 induces chemoresistance in HGSC, we analyzed the expression of genes that p62 regulates as downstream targets of NRF2 signaling, such as *Ho-1* and *Nqo1*, in RPMNP and RPMNP-p62KO cells. The expression of *Ho-1* and *Nqo1* was reduced by the depletion of p62 in RPMNP cells (Fig. 5b and c). Additionally, the expression of *Ho-1* and *Nqo1* in RPMNP cells was downregulated by treatment with EVL (Fig. 5d). The TCGA dataset also indicated that the expression of *HO-1* positively correlated with RAS signaling and PI3K signaling scores according to GSVA (Fig. 5e and f). These results suggest that NRF2 signaling is deregulated downstream of RAS/PI3K-mTOR-p62 signaling. We used Kaplan–Meier plotter to analyze the correlation between the expression of NRF2-downstream genes and prognosis [24]. High levels of *NQO1* and *HO-1* strongly correlated with poor OS and PFS (Fig. 5g–j). Furthermore, after reviewing the significant biological processes in patients with BRCA-WT ovarian cancer analyzed by GSVA (Fig. 1a), we found that the activation of the "cellular response to reactive oxygen species" (ROS) correlated with poor PFS in patients with BRCA-WT ovarian cancer and RAS/PI3K signaling activation (Fig. S5B-D). The upregulated expression of other

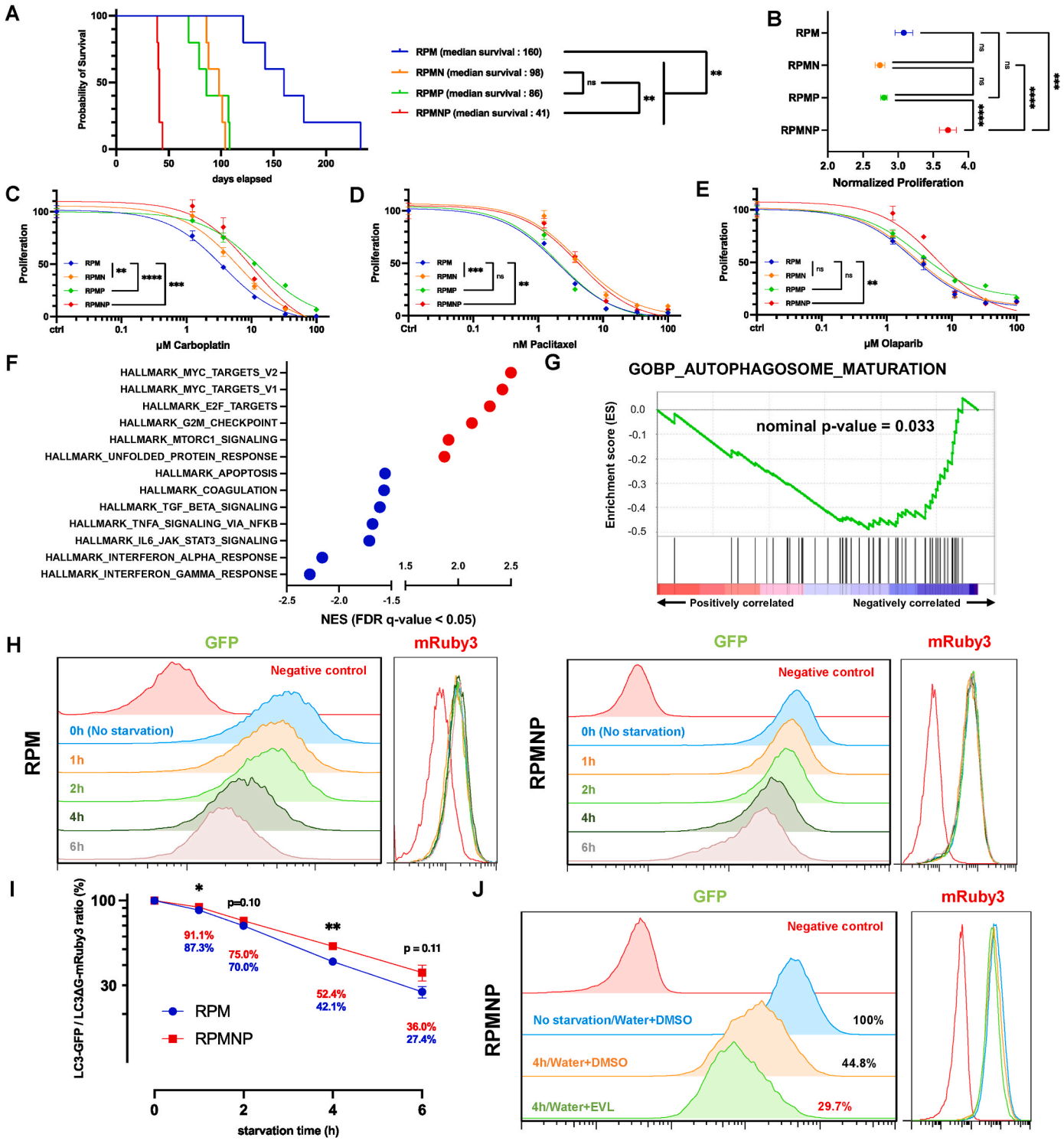

(caption on next page)

Fig. 3. Genotypes activating RAS/PI3K signaling result in poor prognosis and chemoresistance, and inhibit autophagy through mTOR activation.
A, Kaplan–Meier survival curves of nude mice transplanted 1×10^6 RPM (5 mice, blue), RPMN (5 mice, orange), RPMP (5 mice, green), or RPMNP (5 mice, red) cells intraperitoneally in principle. Log-rank test; **B**, Normalized proliferation measured using the CellTiter-Glo 2.0 of RPM, RPMN, RPMP, and RPMNP cells on day 2. Normalization was performed based on the proliferation on day 1. One-way ANOVA test; **C-E**, Dose-response curves of RPM (blue), RPMN (orange), RPMP (green), or RPMNP (red) cells with the treatment of carboplatin (CBDCA, **C**), paclitaxel (PTX, **D**), and Olaparib (**E**). Extra sum-of-squares F test; **F**, RNA-seq analysis by pre-ranked Gene Set Enrichment Analysis (GSEA) indicating enrichment of mSigDB hallmark gene sets in RPMNP cells compared with RPM cells. The y-axis represents gene sets, and the x-axis represents normalized enrichment score (NES); **G**, An enrichment plot and a nominal p-value of an autophagosome maturation pathway depicted by pre-ranked GSEA investigating enrichment of gene sets in biological process ontology in RPMNP cells compared to RPM cells; **H**, Visualization of autophagy flux by flow cytometry of RPM and RPMNP cells transfected with the vector GFP-LC3-mRuby-LC3ΔG. While GFP-labeled LC3 was degraded through autophagy, mRuby-labeled LC3ΔG was stable regardless of the activation of autophagy to be an internal control. After 16 h of culture, the transfected cells were exposed to a culture medium lacking FBS and amino acids; **I**, Relative GFP/mRuby values were normalized, and the control value was measured without starvation. The y-axis indicated relative LC3 degradation by the ratio (%) of relative fluorescence intensity (RFI) of GFP to RFI of mRuby, and the x-axis showed starvation time. The ratios at 0 h (no-starvation, n = 5), 1 h (n = 5), 2h (n = 5), 4 h (n = 5), and 6 h (n = 4) were depicted. Two-tailed student's t-test; **J**, Visualization of autophagy by flow cytometry of RPMNP cells transfected with the vector GFP-LC3-mRuby-LC3ΔG under the treatment with DMSO or an mTOR inhibitor, everolimus. Starvation time was 4 h; *p < 0.05, **p < 0.01, ***p < 0.001, ****p < 0.0001. Data are represented as mean ± SEM, in principle. (For interpretation of the references to color in this figure legend, the reader is referred to the Web version of this article.)

antioxidant genes downstream of NRF2 signaling, such as *GPX4* and *SOD2*, was also correlated with poor PFS in patients with ovarian cancer (Fig. S5E and F). These results suggest that the NRF2-ROS response pathway is upregulated by mTOR-p62 signaling, which is critical for poor progression in patients with ovarian cancer.

3.6. The reinforced mTOR-p62 pathway by chemical-induced NRF2 activation is a potential prognostic biomarker

As a clinical enigma, patients with HGSC are usually initially sensitive to chemotherapy; however, they frequently acquire chemoresistance. We assumed that the mTOR-p62 pathway might be relevant to the acquisition of chemoresistance; therefore, we performed multiplex immunofluorescence analysis of 15 pairs of tumor samples resected before and after neoadjuvant chemotherapy (NAC) from patients with HGSC (PreNAC and PostNAC), including the refractory case mentioned above (Fig. S6A and B; Table 1). According to the immunofluorescence analysis, *BRCA1/2*-mutated HGSC tumors seemed to exhibit slight changes in p62 distribution; however, drastic increases in p62 distribution through NAC were observed in some *BRCA1/2*-WT HGSC tumors (Fig. 6a–c). Importantly, patients with drastic increases in p62 distribution (top 7 patients) had worse PFS than did patients with stable p62 expression (bottom 8 patients) (Fig. 6d). These findings indicated the dynamic distribution of p62 after conventional chemotherapy in HGSC patients, suggesting that the increase in p62 expression in HGSC MRD patients could be a biomarker for poor progression after chemotherapy. Using this sample, we analyzed whether pS6, an aberrant RAS/PI3K signaling activation, could be associated with PFS in 9 patients with *BRCA1/2*-WT HGSC tumors. Although patients with higher pS6 protein levels tended to have poorer PFS, no significant difference was observed, likely due to the limited sample size (Fig. S6C).

The transcription of *SQSTM1* is known to be regulated by NRF2 and to form a positive feedback loop in some cell lines [25]. To investigate the transcriptomic changes in *Sqstm1* following chemotherapy-induced NRF2 signaling activation, we quantified the expression of *Sqstm1* in RPM cells treated with CBDCA at various concentrations; as a result, the transcription of *Sqstm1* was increased by CBDCA treatment in accordance with the activation of NRF2 signaling (Fig. 6e–g). To recapitulate residual disease after chemotherapy in our HGSC model in vivo, we subcutaneously inoculated RPMNP cells into nude mice and administered CBDCA. Platinum treatment increased the expression of p62 and pS6 in subcutaneous tumors (Fig. 6h–k). Furthermore, we validated the upregulation of p62 at the protein level by treatment with CBDCA and found that this upregulation was inhibited by the EVL-induced pharmacological inhibition of mTOR and activation of autophagy (Fig. 6l). These results suggest that the expression of p62 and mTOR signaling are conversely increased by chemotherapy-driven NRF2 signaling activation, which can be blocked by the mTOR inhibitor EVL.

3.7. Refractory HGSC with RAS/PI3K signaling activation harbors therapeutic vulnerability to mTOR inhibition

Taken together, these results showed that aberrant RAS/PI3K signaling activation in *BRCA1/2* WT HGSC worsened patient prognosis via the mTOR-p62-NRF2 pathway, and that conventional chemotherapy increased p62 expression conversely via NRF2 in a transcriptomic manner. Therefore, an mTOR inhibitor has potential as a novel combination remedy for TC treatment. To evaluate the potential of EVL in HGSC, we performed in vitro and in vivo evaluations. Regarding in vitro validation, we compared the sensitivity of RPMNP cells with TC treatment with or without EVL using a colony formation assay. Similar to the combination of EVL and CBDCA, EVL increased the sensitivity of RPMNP cells to TC treatment (Fig. 7a). Considering in vivo validation, we subcutaneously inoculated nude mice with RPMNPs and treated the mice with vehicle, TC, EVL, or EVL supplemented with TC (Fig. 7b). Although the total administration of CBDCA and PTX every 3 weeks did not substantially differ from that of TC treatment in patients with HGSC according to calculated human equivalent volumes, the subcutaneous tumors derived from RPMNP cells exhibited robust resistance to TC treatment on day 31 (Fig. 7c). These findings suggest that the presence of RPMNPs reflects the characteristics of refractory HGSC in humans. Consistent with our in vitro results, combination therapy with EVL and TC had markedly greater antitumor efficacy than did TC treatment alone on day 31. Of note, EVL alone suppressed tumor growth, and the antitumor effect persisted until day 31. However, subcutaneous tumors treated with only EVL started to grow gradually afterwards; on day 40, subcutaneous tumors treated according to the EVL-supplemented TC treatment regimen had the smallest tumor volumes. These in vitro and in vivo findings suggest that the combination of mTOR inhibitors and TC treatment is a powerful therapeutic strategy for chemotherapy-resistant *BRCA1/2* WT HGSC.

4. Discussion

In patients with HGSC, *BRCA1/2* pathogenic variants and homologous recombination defects have been utilized as biomarkers for PARP inhibitors, with reported prolongation of OS and PFS; however, the effects of PARP inhibitors on patients with HGSC with *BRCA1/2* WT or homologous recombination-proficient (HRP) are limited [5,26]. Our findings provide clinically significant insights into HGSC with *BRCA1/2* WT or HRP and could lead to the development of a new classification of patients with HGSC and improve the choice of treatment in patients with refractory conditions. The integration of omics analysis and newly developed HGSC mouse models revealed that aberrant RAS/PI3K signaling activation enhanced resistance to conventional chemotherapy, followed by autophagy failure owing to the activation of mTOR signaling, which resulted in the downstream accumulation of p62 and activation of NRF2 signaling. Validated by murine HGSC organoid

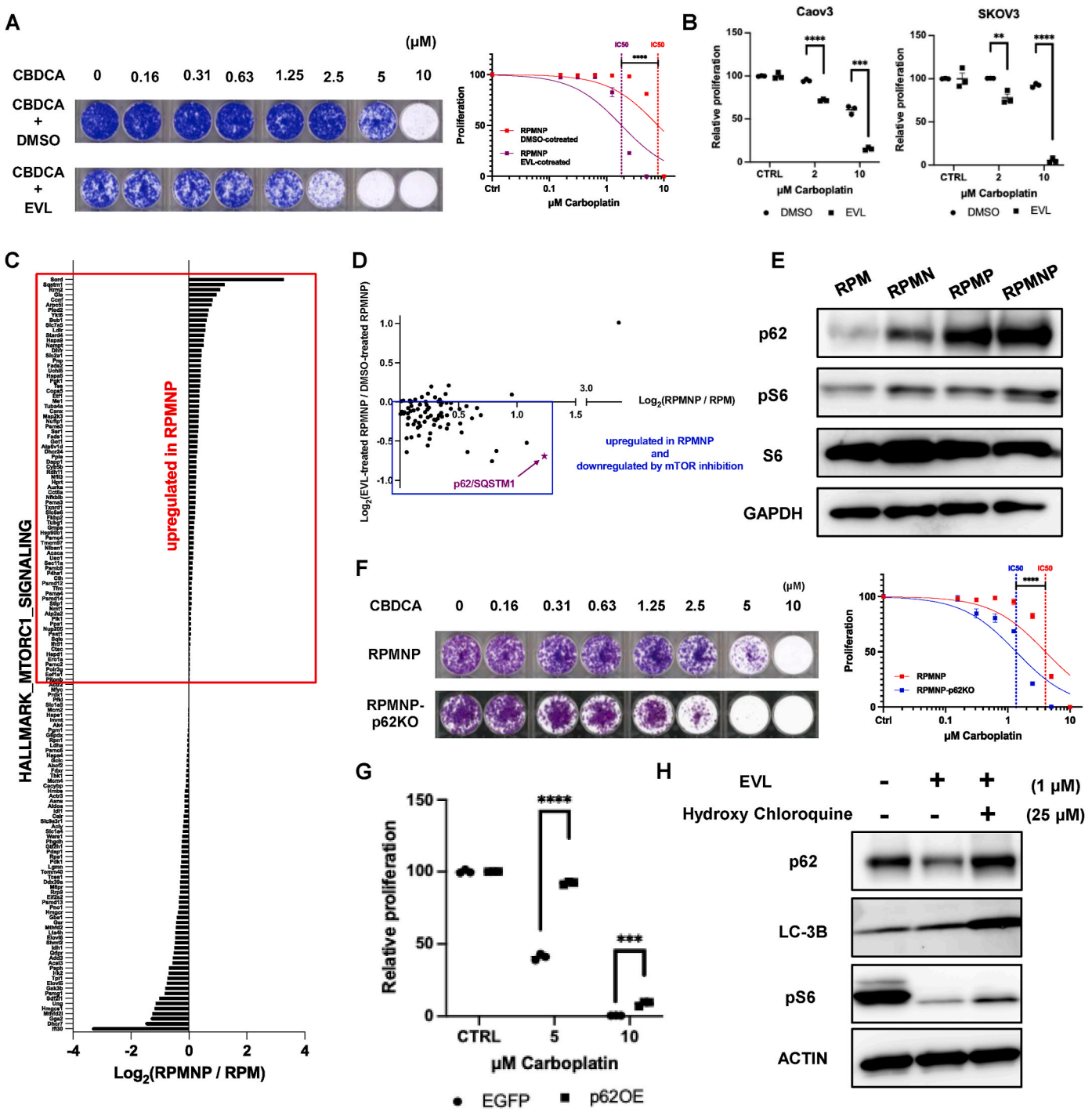

Fig. 4. Pharmacological inhibition of mTORC1 augments an antitumor efficacy of carboplatin to BRCA-WT HGSC by inducing autophagic p62-degradation.

A, Dose–response curves of RPMNP cells treated with CBDCA +0.1 % DMSO, and RPMNP cells treated with CBDCA +100 nM everolimus. Cell viability was measured by crystal violet staining and normalized by cells cultured without CBDCA. Representative stained wells are shown. Extra sum-of-squares F test; **B**, Dose-response quantification of *BRCA1*/2-WT human ovarian cancer cell lines Caov3 and SKOV3. Caov3 and SKOV3 were treated with DMSO, everolimus, 2 μM CBDCA, 2 μM CBDCA and 100 nM EVL, 10 μM CBDCA, and 10 μM CBDCA and 100 nM EVL. Two-talied student's t-test; **C**, A left bar chart represented proteomic expression comparison between RPM cultured with DMSO and RPMNP cultured with DMSO. Proteins included in mSigDB hallmark gene set "mTORC1 signaling" were listed on the y-axis, and upregulated proteins in RPMNP were surrounded by a red box; **D**, A right dot plot represents proteomic expression comparison between RPMNP cultured with DMSO and RPMNP cultured with everolimus. Proteins included in the red box were plotted, and downregulated proteins in EVL-treated RPMNP were surrounded by a blue box; **E**, Western blotting of RPM, RPMN, RPMP, and RPMNP cells. GAPDH, p62, S6, and mTOR signaling activation marker phosphor-S6 (pS6); **F**, Dose-response curves of RPMNP cells with p62 knockout (RPMNP-p62KO) treated with CBDCA compared to that of RPMNP cells. Cell viability was normalized by vehicle-treated cells respectively. Representative stained wells are shown. Extra sum-of-squares F test; **G**, Dose-response quantification of cRPM cells (an *Rb1*$^{-/-}$*Trp53*$^{-/-}$*Myc*^{OE} HGSC model generated in a different way from mFTE cell) overexpressing p62 (cRPM-p62OE) compared to that of cRPM cells expressing EGFP for control. The results with vehicle, 5 μM, and 10 μM CBDCA are shown. Two-tailed student's t-test; H, Western blotting of RPMNP cells treated with vehicle, EVL, both EVL and hydroxychloroquine, which is an autophagy inhibitor. Actin, p62, LC-3B, and pS6; *p < 0.05, **p < 0.01, ***p < 0.001, ****p < 0.0001. Data are represented as mean ± SEM, in principle. (For interpretation of the references to color in this figure legend, the reader is referred to the Web version of this article.)

models and human HGSC tumor samples, the p62 distribution was shown to be a clue for the aggressive phenotype and chemoresistance triggered by the mTOR-p62-NRF2 linkage (Fig. 7d). Although NRF2 signaling is associated with treatment resistance in HGSC, effective therapeutic strategies have not been developed [27]. This study demonstrated that the distribution of p62 was a clue for the aggressive phenotype and chemotherapy resistance caused by the mTOR-p62-NRF2 linkage, and that the use of mTOR inhibitors as a potent strategy against refractory HGSC with increased p62 expression and NRF2 activation could increase p62 degradation and response to TC treatment. Further studies are needed to determine whether p62 could affect invasion and metastasis of HGSC.

In the context of ovarian cancer, the utilization of mTOR inhibitors has been investigated in clinical trials, revealing acceptable toxicity but limited efficacy when used as a monotherapy [28]. A primary challenge is the absence of effective biomarkers. Thus, efforts are ongoing to explore combination therapies, including various mTOR inhibitors and new biomarkers. The dual mTORC1/2 inhibitor vistusertib (AZD2014) has emerged as a prominent candidate for these combination approaches. In a phase I trial (NCT02193633) evaluating the combination of vistusertib and weekly PTX for recurrent/resistant HGSC, the observed overall response rate was encouraging at 52 % (13 of 25 cases). Importantly, despite the absence of significant findings in single gene mutation analysis, a notable discrepancy in *BRCA1/2* mutation rates was observed; the *BRCA1/2* mutation rate of 7.6 % in the partial response arm was markedly lower than that of 30 % observed in the stable disease arm. This observation suggests a potential association between BRCA status and treatment response, implying that the efficacy

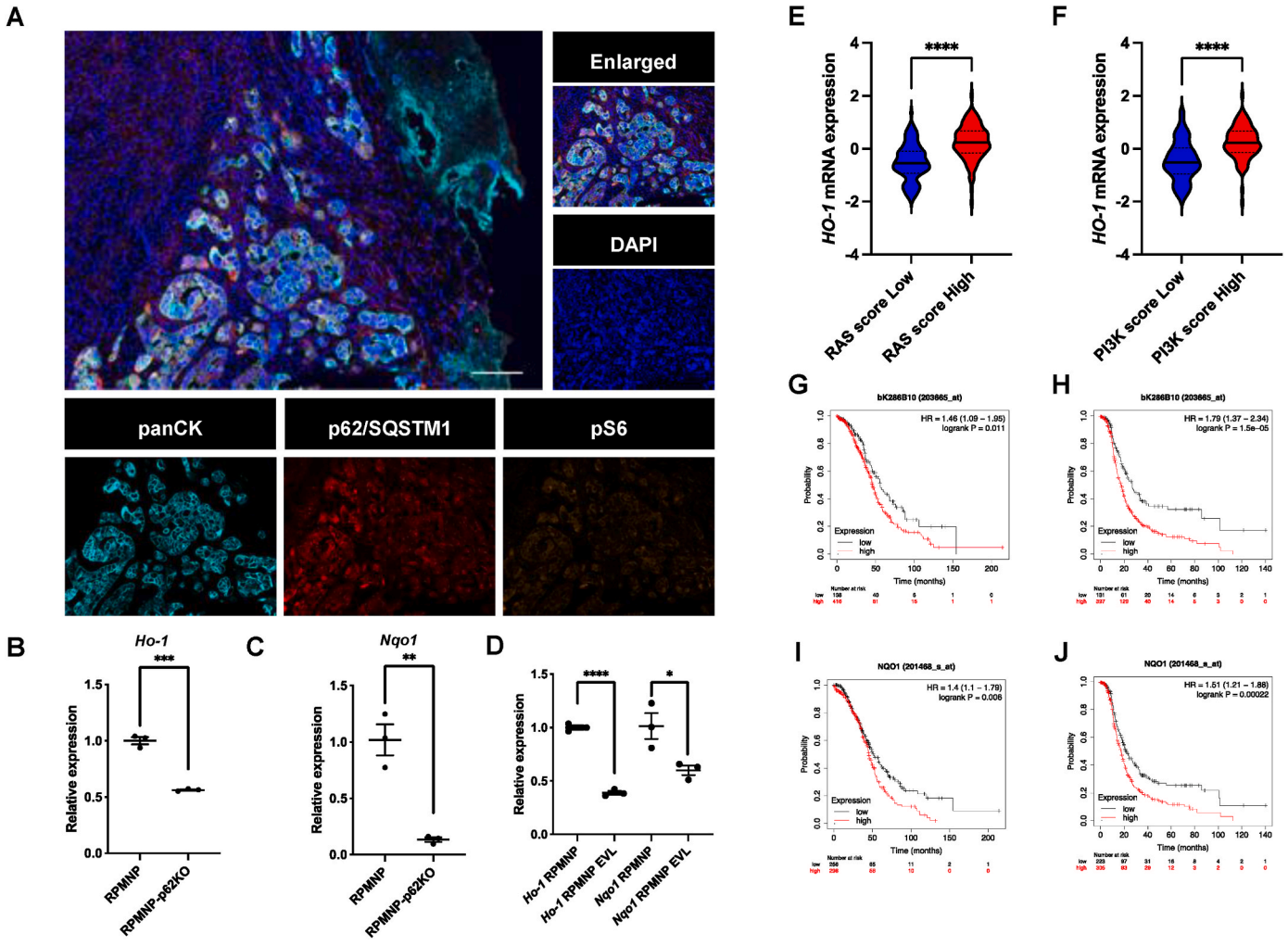

Fig. 5. p62-NRF2 antioxidant pathway activation driven by RAS/PI3K-mTOR, leading to poor prognosis of patients with ovarian cancer.
A, Representative multiplex immunofluorescence of a refractory HGSC tumor sample acquired using Opal Multiplex IHC. An enlarged image and fluorescence-separated images are also shown. Orange: pS6, cyan: CK, red: p62, blue: DAPI. Scale-bar indicated 100 μm; **B**, RNA expression of *Ho-1* in RPMNP and RPMNP-p62KO cells quantified by qPCR. Two-tailed student's t-test; **C**, RNA expression of *Nqo1* in RPMNP and RPMNP-p62KO cells quantified by qPCR. Two-tailed student's t-test; **D**, RNA expression of *Ho-1* and *Nqo1* in RPMNP cells under the treatment with vehicle or 1 μM EVL quantified by qPCR. Two-tailed student's t-test; **E**, Violin plots of RNA expression of *HO-1* in the high RAS-score group and the low group defined in Fig. 1d. Two-tailed student's t-test; **F**, Violin plots of RNA expression of *HO-1* in the high PI3K-score group and the low group defined in Extended Data Fig. 1b. Two-tailed student's t-test; **G**, Kaplan-Meier curves depicted according to *HO-1* (bK286B10) RNA expression and OS of ovarian cancer patients, plotted using "Kaplan-Meier Plotter"; **H**, Kaplan-Meier curves depicted according to *HO-1* (bK286B10) RNA expression and PFS of ovarian cancer patients, plotted using "Kaplan-Meier Plotter"; **I**, Kaplan-Meier curves depicted according to *NQO1* RNA expression and OS of ovarian cancer patients, plotted using "Kaplan-Meier Plotter"; **J**, Kaplan-Meier curves depicted according to *NQO1* RNA expression and PFS of ovarian cancer patients, plotted using "Kaplan-Meier Plotter". *p < 0.05, **p < 0.01, ***p < 0.001, ****p < 0.0001. Data are represented as mean ± SEM, in principle. (For interpretation of the references to color in this figure legend, the reader is referred to the Web version of this article.)

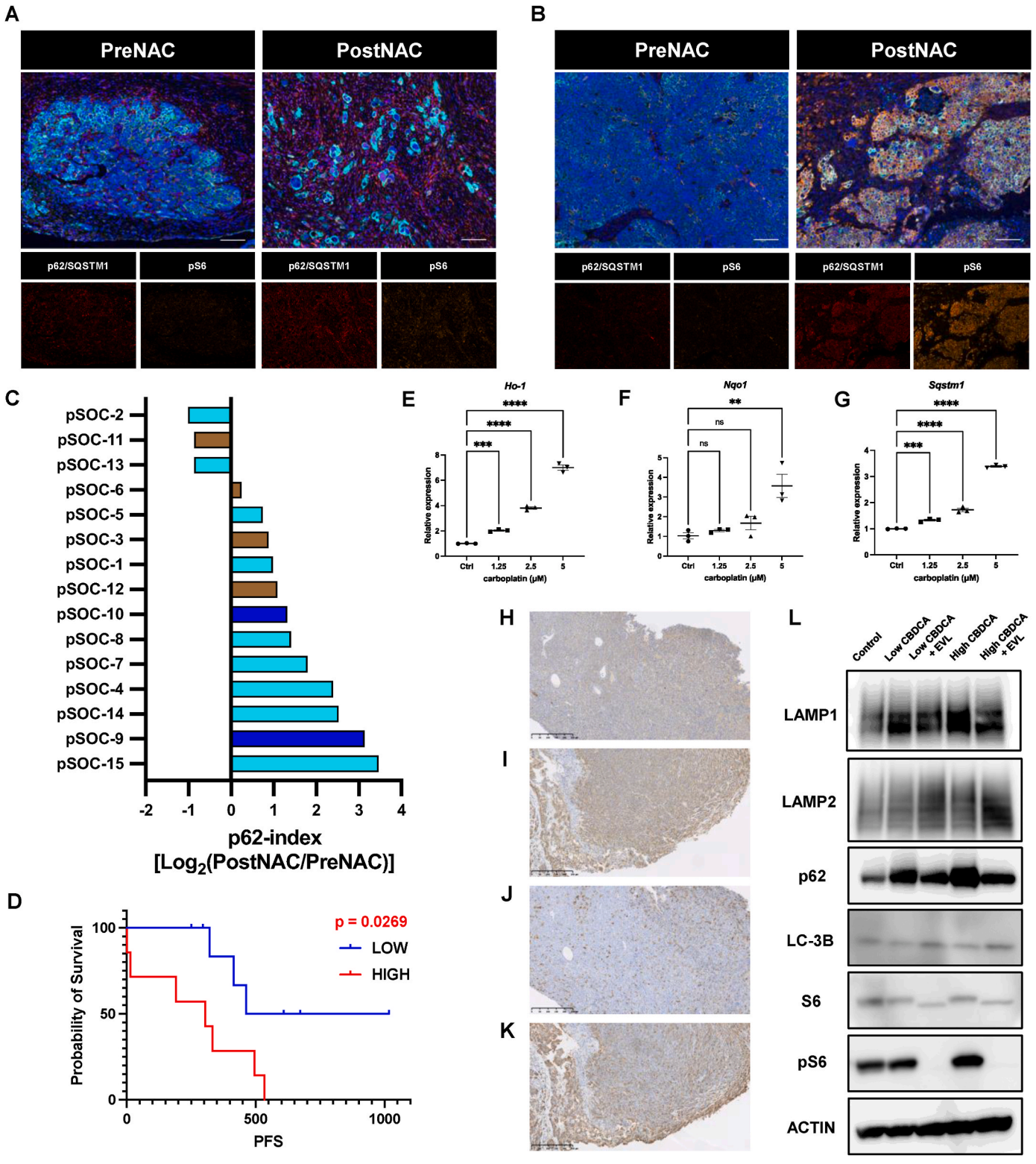

(caption on next page)

Fig. 6. Chemotherapy-induced reinforcement of an mTOR-p62 pathway by NRF2 signaling activation as a potential prognostic biomarker.
A, Representative images of PreNAC and PostNAC HGSC tumor samples of pSOC-6 (*BRCA1/2* mutated HGSC) acquired using Opal Multiplex IHC. Fluorescence-separated images are also shown. Orange: pS6, cyan: CK, red: p62, blue: DAPI. Scale-bars indicated 100 μm; **B**, Representative images of PreNAC and PostNAC HGSC tumor samples of pSOC-8 (*BRCA1/2* WT HGSC) acquired using Opal Multiplex IHC. Fluorescence-separated images are also shown. Orange: pS6, cyan: CK, red: p62, blue: DAPI. Scale-bars indicated 100 μm; **C**, Bar charts of "p62-index" defined by PostNAC/PreNAC ratio of fluorescence intensity of p62 acquired using Opal Multiplex IHC. Cyan bars indicate cases without pathogenic *BRCA1/2* mutation, blue bars indicate cases with genome *BRCA1/2* WT (without tumor genomic profiles), and brown bars indicate cases with pathogenic *BRCA1/2* mutation; **D**, Kaplan-Meier survival curves depicted according to the p62-index and PFS of the HGSC cases. PFS is defined as elapsed days from last platinum date to progression, in principle. (a blue line including cases with the p62-index less than or equal to the median; a red line including cases with the p62-index more than the median). Log-rank test; **E**, RNA expression of *Ho-1* in RPM cells treated with vehicle, 1.25 μM CBDCA, 2.5 μM CBDCA, and 5 μM CBDCA quantified by qPCR. One-way ANOVA test; **F**, RNA expression of *Nqo1* in RPM cells treated with vehicle, 1.25 μM CBDCA, 2.5 μM CBDCA, and 5 μM CBDCA quantified by qPCR. One-way ANOVA test; **G**, RNA expression of *Sqstm1* in RPM cells treated with vehicle, 1.25 μM CBDCA, 2.5 μM CBDCA, and 5 μM CBDCA quantified by qPCR. One-way ANOVA test; **H**, IHC of a subcutaneous tumor sample from an untreated nude mouse stained with p62; **I**, IHC of a subcutaneous tumor sample from a CBDCA-treated nude mouse stained with p62; **J**, IHC of a subcutaneous tumor sample from an untreated nude mouse stained with pS6; **K**, IHC of a subcutaneous tumor sample from a CBDCA-treated nude mouse stained with pS6; **L**, Western blotting of LAMP1, LAMP2, p62, LC-3B, S6, pS6, ACTIN in RPMNP cells. RPMNP cells were treated with nothing, 1.25 μM CBDCA (low), or 2.5 μM CBDCA (high) for the long-term. EVL treatment (1 μM) was for short-term. *$p < 0.05$, **$p < 0.01$, ***$p < 0.001$, ****$p < 0.0001$. Data are represented as mean ± SEM, in principle. (For interpretation of the references to color in this figure legend, the reader is referred to the Web version of this article.)

of this combination therapy may be more pronounced in BRCA WT cases [29]. The OCTOPUS is a phase II randomized clinical trial evaluating whether adding vistusertib to weekly PTX improves PFS and OS in 140 patients with platinum-resistant HGSC [30]. There was a small improvement in PFS (hazard ratio: 0.84) in the experimental arm; however, the biomarker analysis using whole-genome sequencing showed that in the group with copy number signature 4, vistusertib was associated with a significant improvement in PFS and OS in the experimental arm. Copy number signature 4 is predominantly associated with whole-genome duplications and mutations in the PI3K/AKT pathway [30]. This finding was consistent with our data showing that patients with HGSC with mTOR activation had a worse prognosis and that inhibition of the mTOR pathway improved the prognosis.

In this study, we found that EVL, an mTOR inhibitor that stimulates autophagy, inhibited the p62-NRF2 antioxidant defense system and sensitized HGSC model RPMNP cells to conventional chemotherapy. The results showed that EVL, as a single agent, was ineffective against RPMNPs in vitro (Fig. S4A) but had some effect in vivo (Fig. 7c), which could be owing to the timing of treatment. In other words, the mTOR pathway might play an important role in the tumor initiation process before the tumor fully developed, which might have resulted in the tumor-inhibitory effect of EVL-only therapy. However, the tumors eventually relapsed; the single-agent effect was limited.

With regard to autophagy and ovarian cancer treatment, our results are consistent with previous reports stating that the concomitant use of autophagy-promoting agents increases sensitivity to CBDCA in ovarian cancer [31]. However, some reports have shown that in patients with ovarian cancer, the inhibition of autophagy, using agents such as by chloroquine, is effective in combination with chemotherapy. In addition, DIRAS3, a small GTPase that belongs to the RAS superfamily and inhibits RAS function, induces autophagy and is involved in cell dormancy [32,33]. Therefore, the effect of autophagy on cancer cell survival may vary among individuals and under different cell conditions; the evaluation of appropriate biomarkers is necessary for clinical applications. In this study, we found that p62 may be used as a biomarker for assessing mTOR-dependent autophagy defects and is indicated for combination therapy with mTOR inhibitors in appropriate patients.

In summary, by integrating omics analysis and the newly developed *BRCA1/2* WT HGSC mouse model, we found that elevated p62 expression might be a biomarker for poor prognosis. Moreover, combination therapy comprising TC and mTOR inhibitors might be a novel treatment of refractory HGSC. This study could lead to the proposal of a new treatment strategy for managing patients with ovarian cancer with high levels of unmet needs. That is, in patients with advanced ovarian cancer with *BRCA1/2* WT, using cancer tissue collected at the time of interval debulking surgery after neoadjuvant chemotherapy, patients with elevated expression of p62 as a biomarker could be treated with the addition of an mTOR inhibitor as a strategy for increasing the sensitivity of ovarian cancer cells to chemotherapy.

A limitation of this study is that the universality of the biomarkers was not fully demonstrated owing to the limited sample size. Additionally, whether these findings could be applicable to other cancer types remains unclear, including breast cancer. However, further multicenter studies are needed to evaluate biomarkers and patient prognosis across various cancer types. Ultimately, the relationship between biomarkers and treatment efficacy should be further investigated in clinical trials.

CRediT authorship contribution statement

Tomohiro Tamura: Writing – original draft, Visualization, Software, Methodology, Investigation, Formal analysis, Data curation. **Shimpei Nagai:** Visualization, Methodology, Investigation, Data curation. **Kenta Masuda:** Writing – review & editing, Writing – original draft, Visualization, Supervision, Resources, Project administration, Methodology, Funding acquisition, Conceptualization. **Keiyo Imaeda:** Visualization, Investigation, Data curation. **Eiji Sugihara:** Software, Methodology, Investigation, Formal analysis, Data curation. **Juntaro Yamasaki:** Methodology. **Miho Kawaida:** Investigation, Formal analysis. **Yuji Otsuki:** Resources, Methodology. **Kentaro Suina:** Resources, Methodology. **Hiroyuki Nobusue:** Methodology. **Tomoko Akahane:** Investigation. **Tatsuyuki Chiyoda:** Resources. **Iori Kisu:** Resources. **Yusuke Kobayashi:** Resources. **Kouji Banno:** Resources. **Kazuhiro Sakurada:** Resources, Methodology. **Hajime Okita:** Resources. **Rui Yamaguchi:** Software, Methodology. **Ahmed Ashour Ahmed:** Writing – review & editing. **Wataru Yamagami:** Supervision, Resources. **Hideyuki Saya:** Writing – review & editing, Supervision. **Daisuke Aoki:** Supervision, Resources. **Osamu Nagano:** Writing – review & editing, Supervision, Funding acquisition.

5. Research in context

5.1. Evidence before this study

Over 50 % of high-grade serous carcinomas (HGSC) are homologous recombination repair proficient, making patients with HGSC refractory to traditional chemotherapy or poly (ADP-ribose) polymerase (PARP) inhibitors. These patients often develop progressive resistance within 6 months after primary treatment with early-tendency death. However, the molecular mechanisms and therapeutic approach for refractory HGSC with *BRCA1/2* wild-type were not identified.

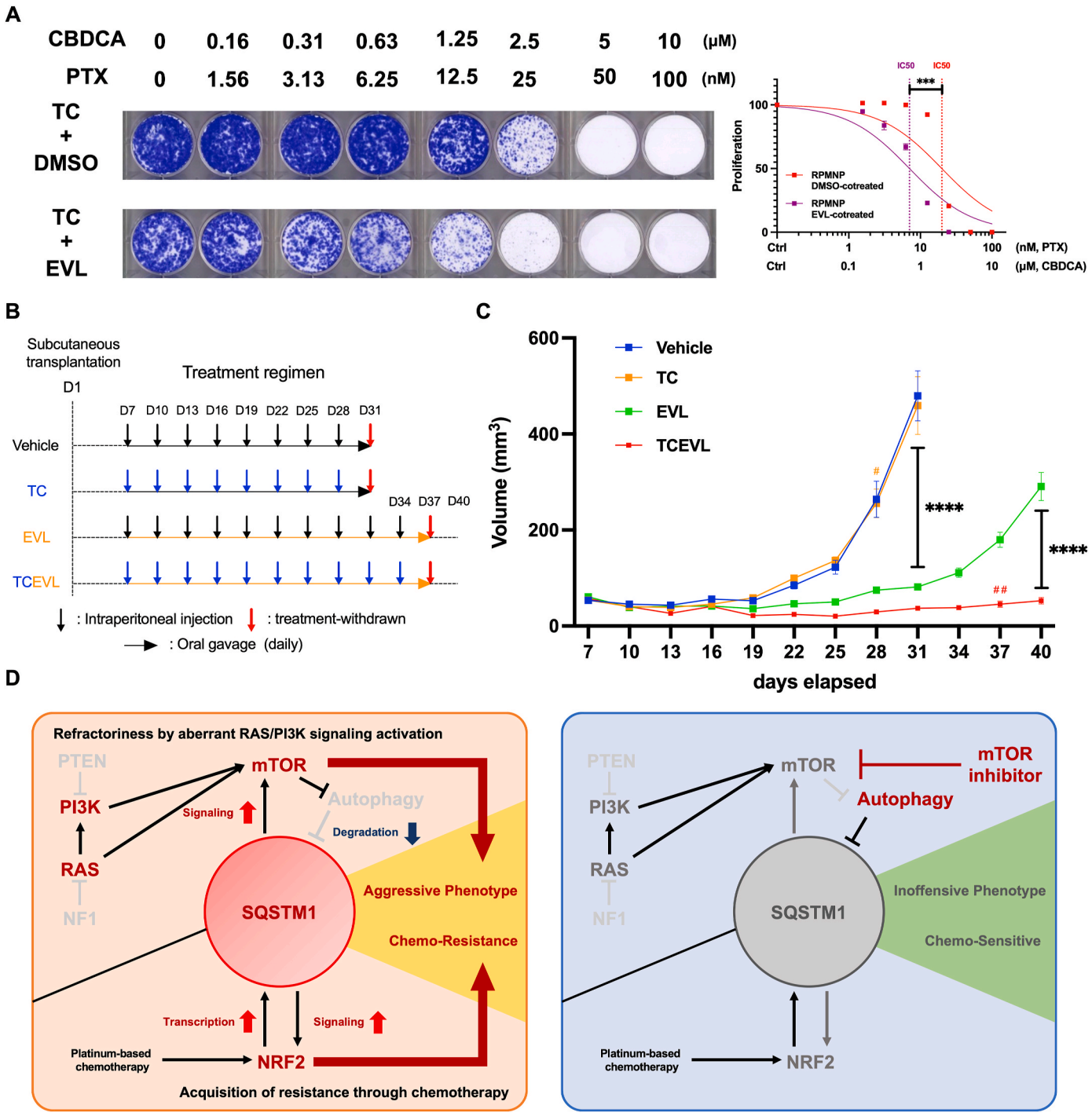

Fig. 7. Impact of the combination therapy of TC treatment and an mTOR inhibitor to HGSC.
A, Dose-response curves of RPMNP cells co-treated with CBDCA, PTX (TC treatment) and DMSO and RPMNP cells co-treated with TC treatment and 100 nM EVL. Cell viability was measured by crystal violet staining and representative stained wells are shown. Extra sum-of-squares F-test; **B**, Treatment regimens in the four groups. Each group started with 5 nude mice receiving bilateral subcutaneous inoculation of 2 × 105 RPMNP cells suspended in 50 μL medium/Matrigel (1:2 v/v) to each flank at day 1, and the tumor volume was evaluated every 3 days from day 7. CBDCA: 30 mg/kg, i.p.; PTX: 8 mg/kg, i.p.; EVL: 5 mg/kg, p.o.; in principle. **C,** Growth curves of subcutaneous tumors under vehicle treatment (blue), TC (orange), EVL (green), or TC and EVL (red). #Incidence of death. Tumor volumes at days 31 and 40 were analyzed statistically by one-way ANOVA test and two-tailed student's t-test, respectively; **D**, Schematic representation of mTORC1-p62-NRF2 linkage and new combinational chemotherapy with TC treatment and an mTOR inhibitor; *p < 0.05, **p < 0.01, ***p < 0.001, ****p < 0.0001. Data are represented as mean ± SEM, in principle. (For interpretation of the references to color in this figure legend, the reader is referred to the Web version of this article.)

5.2. *Added value of this study*

In this study, we comprehensively investigated this tumor type leveraging a combination of machine learning analysis of large published datasets and newly developed genetically engineered models of HGSC formed from murine oviducts. Our findings revealed a previously unrecognized role of mTOR-mediated suppression of autophagy in residual disease following chemotherapy. They also showed that mTOR-induced p62 upregulation was a robust marker for chemotherapy-induced upregulation of mTOR in relevant tumor models and in

patients with ovarian cancer. We found that p62 could act as an important biomarker for therapeutic intervention since mTOR inhibition using everolimus was associated with significant reduction of p62. Finally, using mouse models, our findings showed that treating refractory HGSCs characterized by elevated p62 levels induced robust tumor suppression.

5.3. Implications of all available evidence

The implications of our study are profound, offering novel insights into the molecular mechanisms underlying refractory HGSC with *BRCA1/2* wild-type and providing a promising avenue for developing personalized therapeutic approaches. Elucidating the interplay between RAS/PI3K signaling, autophagy dysregulation, and p62-mediated pathways, we present a prominent case of the integration of mTOR inhibitors with the treatment paradigm for this aggressive malignancy.

Data sharing statement

The RNA-sequencing data have been deposited in the Gene Expression Omnibus (GEO) (RRID:SCR_005012) with GEO accessions GSE255127 and GSE255128.

Funding

This research was supported by AMED under Grant Number JP23ama221509, JSPS KAKENHI Grant Numbers JP20K18174 and JP23K06640, the Kobayashi Foundation for Cancer Research, Keio Gijuku Academic Development Funds (to K.M.), Keio University Medical Science Fund (to K.M. and T.T.), and the Moonshot R&D-MILLENNIA Program (JPMJMS2022-19 to O.N.) of the Japan Science and Technology Agency.

Declaration of competing interest

The authors declare the following financial interests/personal relationships which may be considered as potential competing interests: K. M. is filing a patent application for the use of the biomarker, method of determining prognosis, and therapeutic agent for ovarian cancer and has received lecture fees from AstraZeneca and Takeda Pharmaceutical. Y.K. has received lecture fees from AstraZeneca and Takeda Pharmaceutical. W.Y. has received lecture fee from AstraZeneca and Merck & Co., Inc. AAA is a founder, director and scientific adviser for Singula Bio. D.A. has received lecture fee from Chugai Pharmaceutical, AstraZeneca, Myriad Genetics, MSD, Taiho Pharmaceutical, and Takeda Pharmaceutical and payment for expert testimony from Chugai Pharmaceutical and MSD.

Acknowledgement

We thank the Core Facility, Collaborative Research Resources and JSR-Keio University Medical and Chemical Innovation Center (JKiC) for help with the experiments. The authors thank Dr. N. Mizushima and Dr. H. Chino for kindly providing the plasmid vector and A. Aoki, H. Nakazawa, and I. Ishimatsu for their kind assistance. The GFP-LC3-mRuby3-LC3ΔG vector was kindly provided by N. Mizushima and H. Chino of The University of Tokyo.

This research was supported by AMED under Grant Number JP23ama221509, JSPS KAKENHI Grant Numbers JP20K18174 and JP23K06640, the Kobayashi Foundation for Cancer Research, Keio Gijuku Academic Development Funds (to K.M.), Keio University Medical Science Fund (to K.M. and T.T.), and the Moonshot R&D-MILLENNIA Program (JPMJMS2022-19 to O.N.) of the Japan Science and Technology Agency.

Glossary

CBDCA, carboplatin; TCGA, Cancer Genome Atlas; EVL, everolimus; HRD, homologous recombination deficiency; HRP, homologous recombination-proficient; FFPE, formalin and paraffin embedded; GSEA, gene set enrichment analysis; GSVA, gene set variation analysis; HGSC, High-grade serous carcinoma; IHC, immunohistochemistry; IF, immunofluorescence; MRD, minimal residual disease; NAC, neo-adjuvant chemotherapy; OS, overall survival; OE, overexpression; PTX, paclitaxel; PARP, poly(ADP-ribose) polymerase; TC, CBDCA + PTX; PFS, progression-free survival; ROS, reactive oxygen species; WES, whole exome sequencing; WT, wild type.

Appendix A. Supplementary data

Supplementary data to this article can be found online at https://doi.org/10.1016/j.canlet.2025.217565.

References

[1] D.D. Bowtell, S. Böhm, A.A. Ahmed, P.-J. Aspuria, R.C. Bast, V. Beral, et al., Rethinking ovarian cancer II: reducing mortality from high-grade serous ovarian cancer, Nat. Rev. Cancer 15 (2015) 668–679.
[2] S. Lheureux, C. Gourley, I. Vergote, A.M. Oza, Epithelial ovarian cancer, Lancet 393 (2019) 1240–1253.
[3] P. Disilvestro, S. Banerjee, N. Colombo, G. Scambia, B.G. Kim, A. Oaknin, et al., Overall survival with maintenance olaparib at a 7-year follow-up in patients with newly diagnosed advanced ovarian cancer and a BRCA mutation: the SOLO1/GOG 3004 Trial, J. Clin. Oncol. 41 (2023) 609–617.
[4] K. Moore, N. Colombo, G. Scambia, B.-G. Kim, A. Oaknin, M. Friedlander, et al., Maintenance olaparib in patients with newly diagnosed advanced ovarian cancer, N. Engl. J. Med. 379 (2018) 2495–2505.
[5] I. Ray-Coquard, P. Pautier, S. Pignata, D. Pérol, A. González-Martín, R. Berger, et al., Olaparib plus bevacizumab as first-line maintenance in ovarian cancer, N. Engl. J. Med. 381 (2019) 2416–2428.
[6] D. Yang, S. Khan, Y. Sun, K. Hess, I. Shmulevich, A.K. Sood, et al., Association of BRCA1 and BRCA2 mutations with survival, chemotherapy sensitivity, and gene mutator phenotype in patients with ovarian cancer, JAMA 306 (2011) 1557–1565.
[7] D.J. Gallagher, J.A. Konner, K.M. Bell-McGuinn, J. Bhatia, P. Sabbatini, C. A. Aghajanian, et al., Survival in epithelial ovarian cancer: a multivariate analysis incorporating BRCA mutation status and platinum sensitivity, Ann. Oncol. 22 (2011) 1127–1132.
[8] D. Bell, A. Berchuck, M. Birrer, J. Chien, D.W. Cramer, F. Dao, Integrated genomic analyses of ovarian carcinoma, Nature 474 (2011) 609–615.
[9] A.M. Patch, E.L. Christie, D. Etemadmoghadam, D.W. Garsed, J. George, S. Fereday, et al., Whole-genome characterization of chemoresistant ovarian cancer, Nature 521 (2015) 489–494.
[10] M. Artibani, K. Masuda, Z. Hu, P.C. Rauher, G. Mallett, N. Wietek, et al., Adipocyte-like signature in ovarian cancer minimal residual disease identifies metabolic vulnerabilities of tumor-initiating cells, JCI Insight 6 (2021).
[11] S. Hänzelmann, R. Castelo, J. Guinney, GSVA: gene set variation analysis for microarray and RNA-Seq data, BMC Bioinf. 14 (2013) 7.
[12] D.P. Bondeson, B.R. Paolella, A. Asfaw, M.V. Rothberg, T.A. Skipper, C. Langan, et al., Phosphate dysregulation via the XPR1–KIDINS220 protein complex is a therapeutic vulnerability in ovarian cancer, Nat. Can. (Ott.) 3 (2022) 681–695.
[13] P. Goossens, J. Rodriguez-Vita, A. Etzerodt, M. Masse, O. Rastoin, V. Gouirand, et al., Membrane cholesterol efflux drives tumor-associated macrophage reprogramming and tumor progression, Cell Metab. 29 (2019) 1376–1389.e4.
[14] K. Levanon, V. Ng, H.Y. Piao, Y. Zhang, M.C. Chang, M.H. Roh, et al., Primary ex vivo cultures of human fallopian tube epithelium as a model for serous ovarian carcinogenesis, Oncogene 29 (2010) 1103–1113.
[15] R.J. Platt, S. Chen, Y. Zhou, M.J. Yim, L. Swiech, H.R. Kempton, et al., CRISPR-Cas9 knockin mice for genome editing and cancer modeling, Cell 159 (2014) 440–455.
[16] A. Subramanian, P. Tamayo, V.K. Mootha, S. Mukherjee, B.L. Ebert, M.A. Gillette, et al., Gene set enrichment analysis: a knowledge-based approach for interpreting genome-wide expression profiles, Proc. Natl. Acad. Sci. U. S. A. 102 (2005) 15545–15550.
[17] Z.A. Abdelhamed, T.A. Ryan, M. Fuller, C. Coulson-Gilmer, D.I. Abdelmottaleb, T. L. Wang, et al., Characterization of primary cilia in normal Fallopian tube epithelium and serous tubal intraepithelial carcinoma, Int. J. Gynecol. Cancer 28 (2018) 1535–1544.
[18] G. Mollaoglu, M.R. Guthrie, S. Böhm, J. Brägelmann, I. Can, P.M. Ballieu, et al., MYC drives progression of small cell lung cancer to a variant neuroendocrine subtype with vulnerability to Aurora kinase inhibition, Cancer Cell 31 (2017) 270–285.
[19] G. Kroemer, G. Mariño, B. Levine, Autophagy and the integrated stress response, Mol. Cell 40 (2010) 280–293.

[20] T. Kaizuka, H. Morishita, Y. Hama, S. Tsukamoto, T. Matsui, Y. Toyota, et al., An autophagic flux probe that releases an internal control, Mol. Cell 64 (2016) 835–849.
[21] S. Domcke, R. Sinha, D.A. Levine, C. Sander, N. Schultz, Evaluating cell lines as tumour models by comparison of genomic profiles, Nat. Commun. 4 (2013) 2126.
[22] Y. Ichimura, S. Waguri, Y.S. Sou, S. Kageyama, J. Hasegawa, R. Ishimura, et al., Phosphorylation of p62 activates the Keap1-Nrf2 pathway during selective autophagy, Mol. Cell 51 (2013) 618–631.
[23] R. Iwadate, J. Inoue, H. Tsuda, M. Takano, K. Furuya, A. Hirasawa, et al., High expression of SQSTM1/p62 protein is associated with poor prognosis in epithelial ovarian cancer, Acta Histochem. Cytoc. 47 (2014) 295–301.
[24] B. Győrffy, Discovery and ranking of the most robust prognostic biomarkers in serous ovarian cancer, GeroScience 45 (2023) 1889–1898.
[25] A. Jain, T. Lamark, E. Sjøttem, K.B. Larsen, J.A. Awuh, A. Øvervatn, et al., p62/SQSTM1 is a target gene for transcription factor NRF2 and creates a positive feedback loop by inducing antioxidant response element-driven gene transcription, J. Biol. Chem. 285 (2010) 22576–22591.
[26] A. González-Martín, B. Pothuri, I. Vergote, R. DePont Christensen, W. Graybill, M. R. Mirza, et al., Niraparib in patients with newly diagnosed advanced ovarian cancer, N. Engl. J. Med. 381 (2019) 2391–2402.
[27] J. Helleman, M. Smid, M.P.H.M. Jansen, M.E.L. van der Burg, E.M.J.J. Berns, Pathway analysis of gene lists associated with platinum-based chemotherapy resistance in ovarian cancer: the big picture, Gynecol. Oncol. 117 (2010) 170–176.
[28] G. Emons, C. Kurzeder, B. Schmalfeldt, P. Neuser, N. De Gregorio, J. Pfisterer, et al., Temsirolimus in women with platinum-refractory/resistant ovarian cancer or advanced/recurrent endometrial carcinoma. A phase II study of the AGO-study group (AGO-GYN8), Gynecol. Oncol. 140 (2016) 450–456.
[29] B. Basu, M.G. Krebs, R. Sundar, R.H. Wilson, J. Spicer, R. Jones, et al., Vistusertib (dual m-TORC1/2 inhibitor) in combination with paclitaxel in patients with high-grade serous ovarian and squamous non-small-cell lung cancer, Ann. Oncol. 29 (2018) 1918–1925.
[30] S. Banerjee, G. Giannone, A.R. Clamp, D.P. Ennis, R.M. Glasspool, R. Herbertson, et al., Efficacy and safety of weekly paclitaxel Plus vistusertib vs paclitaxel alone in patients with platinum-resistant ovarian high-grade serous carcinoma: the OCTOPUS multicenter, Phase 2, randomized clinical trial, JAMA Oncol. 9 (2023) 675–682.
[31] A. Khurana, D. Roy, E. Kalogera, S. Mondal, X. Wen, X. He, et al., Quinacrine promotes autophagic cell death and chemosensitivity in ovarian cancer and attenuates tumor growth, Oncotarget 6 (2015) 36354–36369.
[32] Z. Lu, M.T. Baquero, H. Yang, M. Yang, A.S. Reger, C. Kim, et al., DIRAS3 regulates the autophagosome initiation complex in dormant ovarian cancer cells, Autophagy 10 (2014) 1071–1092.
[33] Z. Lu, R.Z. Luo, Y. Lu, X. Zhang, Q. Yu, S. Khare, et al., The tumor suppressor gene ARHI regulates autophagy and tumor dormancy in human ovarian cancer cells, J. Clin. Investig. 118 (2008) 3917–3929.